TAMPERE UNIVERSITY OF TECHNOLOGY
Department of Biomedical Engineering

NERISHO SEYOUM GETACHEW

THE EFFECT OF MAGNETIC RESONANCE IMAGING SEQUENCE ON THE DETECTION OF LYMPHOMAS

Master of Science Thesis

Supervisors: Professor Hannu Eskola and Xingchen Wu (Dr)
Subject and Supervisors approved by the Faculty Council of the Faculty of Science and Environmental Engineering on 11 January 2012.

ABSTRACT

TAMPERE UNIVERSITY OF TECHNOLOGY
Master's Degree Programme in Biomedical Engineering
Nerisho, Seyoum Getachew, The effect of magnetic resonance imaging sequence on the detection of lymphomas.
Master of Science Thesis, 52 pages.
January 2012
Major subject: Medical Physics
Examiner: Professor Hannu Eskola
Keywords: Non-Hodgkin's lymphoma (NHL), diffuse large B-cell lymphoma, DLBCL, Magnetic resonance imaging, MRI, response to chemotherapy.

Because of its superior sensitivity toward soft tissues, including neoplasm, MRI imaging is rapidly becoming one of preferred imaging modality. Improving the sensitivity of MRI for the detection of aggressive lymphomas, DLBCL, is vital in the diagnostic workup, staging and treatment planning. It is also useful for the better understanding of treatment outcomes in the disease follow-up process.

In this study, the sensitivity of the four MRI sequences, before and after treatment, in delineating the lesion and evaluating the response to treatment is studied.

Eighteen patients with histologically proven DLBCL underwent a 3T MR scanning before treatment, and fifteen of them were re-scanned one week after chemotherapy. The four MRI sequences studied are pre and post contrast enhanced T_1-weighted imaging, T_2-weighted imaging with and without fat suppression. Before treatment all but one patient had not had T_2-weighted fat suppression MRI protocol. The four MRI sequence were quantitatively evaluated based on the normalized mean signal intensity calculated from the measured signal intensities of the lesion and normal tissues.

The conspicuity level of the tumor was superior on T_2-weighted with fat suppression images both before and after treatment. And these difference were significant ($p<0.05$). The post contrast enhanced images ranked the second. One week after treatment, there were a significant decrease in the signal contrast ratio of the T_2-weighted with fat suppression images whereas there were no significant decrease in the signal contrast ratio of the post contrast enhanced T_1-weighted images.

T_2-weighted with fat suppression sequence is the best for detecting lymphoma lesions and evaluating treatment efficacy in patients with DLBCL.

PREFACE

This Master of Science thesis is carried out at Tampere University Hospital in the Department of Biomedical Engineering, Tampere University of Technology,Tampere, Finland.

Firstly, I would like to thank God for letting me pass safely in difficult moments. I would also like to express my sincere gratitude to my supervisors, Prof. Hannu Eskola and Dr. Xingchen Wu for giving me the opportunity to work, for their time and guidance throughout on my thesis. I also thanks to Pertti Ryymin for his valuable advices and time. I also thanks to Prasun Dastidar for his comments and time. Moreover I would like to thank my friends who were there whenever I need their help. Finally I would like to express my greatest thanks to my family whom I do not get a word to describe their help.

Tampere, January 2012

NERISHO SEYOUM GETACHEW

0443620026/0442039524

Table of contents

LIST OF SYMBOLS AND ABBREVIATIONS

ADC	Apparent Diffusion coefficient
CE	Contrast enhanced
CNS	Central nervous system
CSF	Cerebrospinal fluid
CT	Computed tomography
DLBCL	Diffused large B cell lymphoma
DWI-MRI	Diffusion-weighted imaging
EPI	Echo planner imaging
ETL	Echo train length
FDG	Fluorine -18-Fludeoxyglucose
FID	Free induction decay
FLAIR	Fluid-attenuated inversion-recovery
FNA	Fine needle aspirate
fs	Fat suppression
FSE	Fast Spin echo
GD-DTPA	Gadolinium- diethylene triamine pentaacetic acid
GRE	Gradient echo
HAST	Half-Fourier single-shot turbo spin echo
HL	Hodgkin lymphoma
ICD-O	International Classification of Disease-oncology
M	Magnetization vector
M_{xy}	Transverse magnetization vector
M_z	Longitudinal magnetization vector
NHL	Non-Hodgkin lymphoma
PACS	Picture Archiving and Communication System,

PET	Positron Emission Tomography
REAL	Revised European American classification of the lymphoid neoplasm
RF	Radio frequency
ROI	Region of interest
SE	Spin echo
SNR	Signal to noise ratio
STIR	Short tau-inversion-recovery
SUV	Standardize uptake value
TE	Echo times
TSE	Turbo spin echo
TR	Pulse repetition times
T_1	Spin–lattice relaxation time
T_1C	Post contrast enhanced T_1
T_2	Spin–spin relaxation time
T^*_2	T*2 relaxation time
VIBE	Volumetric interpolated breath-hold examination
WB-MRI	Whole body magnetic resonance imaging
WHO	World Health Organization
2D	Two-dimensional
3D	Three dimensional

1. INTRODUCTION

In clinical diagnoses of patients, imaging has become an important tool in the detection and diagnosis of pathological changes. Certain diseases are so critical that early detection and diagnosis are important in prescribing proper treatment. One area where imaging plays a crucial role is on cancer studies.

Lymphoma is a type of blood cancer that appears when lymphocytes start to duplicate faster than a normal cell or live longer than a normal lymphocyte. Lymphoma is divided into two sub groups: Hodgkin lymphoma (HL) and non-Hodgkin lymphoma (NHL). In Finland, as per Finnish Cancer Registry, lymphoma in male and female is the fifth and sixth most frequent neoplasias respectively. The statistics also predicts that lymphoma belongs to a class of malignancies with noticeable increase in occurrence with time. But, due to the current and future advancement in early cancer diagnosis, treatment, and follow-up, the detection of cancer in future may be different. Various radiological imaging modalities have been used for cancer staging, treatment planning and evaluation of response to treatments. And for the better outcome of the treatment and follow-up of patients with HDL and NHL, a precise staging and treatment planning using multidisciplinary approach is a must. Poorly over-staged malignancy may result in unnecessary use of aggressive chemotherapy and beam radiation which could lead to development of secondary malignancy.

Computed tomography (CT) is one of the most commonly used cross-sectional imaging modality in the clinical application of early diagnosis and staging of lymphoma [1]. As to diagnostic efficiency, CT has a good anatomical resolution, but it has lower performance in detecting pathological changes in normal-sized tissue structures; it is a challenge to differentiate residual malignancy from fibrosis and also does not have a good resolution towards soft tissue structures. In addition, in CT there is a possibility to expose patients to higher radiation dose. As metabolic characteristic of a tissue has become more vital in cancer studies, positron emission tomography (PET) using 2 [fluorine-18]-fluoro-2-deoxy-D-glucose (FDG) has become an essential technique in enhancing the staging and follow-up process, and for studying the function of the disease behavior in clinical oncology [2,3,4]. The most peculiar advantage of this method is that it can provide the metabolic information of the malignant tissue which can be used for the analysis of the degree of cancer, the response to treatment and for early detection of disease recurrence, i.e., cancerous tissues with normal tissue sizes can easily be detected by their metabolic activities on the PET image [5, 6, 7]. One of the most pronounced disadvantages of PET is that it has low spatial resolution as a result of which it is less likely to detect small metastatic nodes (nodes < 4 mm) [8]. Recently, fused

FDG-PET/CT has emerged as a very important imaging modality in lymphoma studies by providing high anatomic information from CT which is complemented by metabolic information from PET, i.e., cancer cell metabolize glucose much greater than the surrounding structures [9], which gives visual and semiquantitative information on the PET/CT. This makes PET/CT information to be more accurate than PET or CT each alone [10]. In spite of this, PET/CT is found to be expensive in routine clinical application [11], and the fact that it has radiation exposure risks to patients which may subsequently cause radiation-related cancer [12, 13] makes it not highly applicable as it is considered to be.

Nowadays, magnetic resonance imaging (MRI) is emerging as a promising technique in lymphoma studies because of the fact that MRI enables to provide different tissue structures with high contrast and spatial resolution for an accurate visualization of internal structure, which are vital in diagnosis, staging and follow-up of cancer, without risking the patient to radiation exposure related malignancies and iodinated, potential nephrotoxic contrast agents. The different MRI sequences make the modality to be applicable in broad areas of tissue structures. The conventional T_1 and T_2-weighted imaging sequences, the most commonly used sequences for soft tissue and related diseases, could alone give a lot of information about the target being studied. In addition, recent improvement in MRI technology, such as, multi-channel phased array surface coils and parallel imaging acquisition, has made a high-spatial-resolution and whole-body MRI (WB-MRI) examination possible in a much less imaging time than as it used to be before [14]. Especially, lymphomas, such as non-Hodgkin lymphoma (NHL), are so aggressive that they can metastasize the whole body, and in such a metastatic situation, the role of WB-MRI is crucial [15]. Different MR image analysis techniques, such as volumetric MR image analysis and MRI texture analysis have been studied and found to be promising in treatment response monitoring and evaluation [16, 17]. Moreover, specialized MRI techniques, such as, diffusion-weighted imaging (DWI) with apparent diffusion coefficient (ADC) mapping, are able to provide functional imaging of tissue structures that let MRI to be applied in the early detection of cancerous tumor tissues and to discriminate malignant from benign or differentiate residual malignancy from fibrosis or necrosis [18].

The aim of the thesis is to compare the conspicuity of the most common NHL, DLBCL, on the T_1-weighted imaging before and after contrast medium (Gadolinium) injection, T_2-weighted imaging with and without fat suppression and to analyze the changes between the MRI sequences before and after one week treatment.

2. THEORETICAL BACKGROUND

2.1. Non-Hodgkin lymphoma (NHL)

Lymphomas are heterogeneous group of malignancies that are estimated to account for approximately 3-4% of cancers worldwide and are more frequent in males (3.8%) than in females (3%) [19]. It occurs when lymphocytes duplicate abnormally. Our body has two main types of lymphocytes that can develop into lymphomas: B-lymphocytes (B-cells) and T-lymphocytes (T-cells). These cancerous cells can travel to different parts of the body, such as, lymph nodes, liver, bone marrow, spleen, blood, and can conglomerate to form tumors. There are two main categories of lymphomas: Hodgkin lymphoma (HL) and non-Hodgkin lymphoma (NHL). NHLs are the most frequent lymphomas worldwide [19].

2.1.1. Etiology of non-Hodgkin lymphoma

Etiology of NHL is not clearly known. Studies show that it is highly probable that NHL evolve from conditions that can genetically disorder the DNA function of a cell. HIV/AIDS and organ transplantation have the potential to result in dysfunction of T-cell that can result in EBV driven B-cell proliferation [20, 21].

2.1.2. Biology of non-Hodgkin lymphoma

Most of the NHLs originate from B lymphocytes at various stages of differentiation of the B cells within the lymphoid tissues called central and peripheral lymphoid tissues. Because of the cytogenetic activities, this differentiation of B cells in the lymphoid tissues may result in changes in the cytological working principles. An abnormal cytogenetic activity can result in the activation of proto-oncogene and disorder in the tumour suppressor genes. The translocation of the chromosomes is one of the main mechanisms for the activation of the proto-oncogene. This activation of proto-oncogene has the potential to produce a cancerous cell [22, 23, 24].

2.1.3. Histology of non-Hodgkin lymphoma

NHLs are a group of heterogeneous malignancies of the lymphoid system. The various clinical behaviors, prognoses, origins and the continuous finding of new information about the NHL have resulted in their classification to be changing through years. The revised European American classification of the lymphoid neoplasm, REAL classification, which was published in 1993 by the international lymphoma study group, consisting of outstanding histopathologists from USA,

Europe, and Asia, has been widely used. The reproducibility between pathologists, finding of new disease types with different clinical behaviors, and validity of the REAL classification have been assessed through an accurate clinical environment, and its positive outcomes have made the classification to be accepted by the oncologists. The REAL classification is updated by WHO and now known as to the WHO classification. The WHO classification system is integrated to the newest edition of the coding system called the International Classification of Disease-Oncology (ICD-O). Based on this classification, ICD-O, histological groups of NHL are: B-lymphocytic lymphoma, lymphoplasmacytic lymphoma, mantle cell lymphoma, mixed small/large cell diffuse lymphoma, large B-cell diffuse lymphoma, Burkitt's lymphoma, follicular grade 2 lymphoma, follicular grade 3 lymphoma, all follicular combined, marginal zone, mycosis fungicides/sezary's syndrome, other mature T-cell lymphomas, angioblastic T-cell, cutaneous T-cell, anaplastic T-cell, other T-cell, NK/null cell, precursor B-cell lymphoma/leukemias, and unspecified lymphomas [24, 25, 26, 27]. Broadly NHL is classified into two categories: B-cell lymphomas (accounts approximately 85% of NHLs and develop from abnormal B lymphocytes) and T-cell lymphomas (accounts approximately 15% of NHLs and develop from abnormal T lymphocytes). Follicular lymphoma and diffuse large B-cell lymphoma (DLBC) are the two most common B-cell NHL [28, 29]. In this work, we are dealing with patients with DLBC lymphoma. DLBC NHL can be diagnosed in any age group but are more frequent in older people. It usually starts from lymph nodes, such as, lymph nodes of the chest and abdomen, and it can also appear in the intestine, bone, brain and spinal cord too. Localized DLBC lymphomas account for 33%, and this makes their treatment much easier and has a better prognosis than non-localized one. Even if DLBC NHLs are fast growing lymphoma types, their response to treatment is very good [27].

2.1.4. Signs and Clinical Symptoms of non-Hodgkin lymphoma

The most common symptoms are: enlarged lymph nodes on the side of the neck and collar bones; swollen abdomen due to the enlarged lymph nodes in the stomach that can cause pain and appetite loss; and pain in the chest area due to the presence of lymphoma in the thymus which result in pain and difficulty in breathing because of pressure in the chest (trachea). NHL can also affect the brain, and symptoms, such as, headache, thinking problem, personality change, and vision problems can also occur [27].

2.1.5. Staging of non-Hodgkin Lymphoma

Once the symptoms of NHLs are recognized, a number of diagnostic methods are used. After diagnosis of lymphoma is made, it has to be graded appropriately so that patients are grouped in the right category that would facilitate to plan a better

treatment, predict the likelihood of the response and outcome of the proposed treatment plan. The standard staging of NHL is based on the Ann Arbor staging system, table.1. The Ann Arbor staging system was primarily designed for HL and has some limitations in the staging of NHL. Thus the Ann Arbor staging is not important in NHL as it is in HL [30, 31].

Table1. The modified Ann Arbor staging system for NHL

Stage	Characteristics
I	Involvement of a single lymph node region
II	Involvement of two or more lymph node regions on the same side of the diaphragm
III	Involvement of lymph node regions on both sides of the diaphragm
IV	Extra nodal organ involvement
A	Absence of constitutional symptoms
B	Presence of constitutional symptoms
E	Extranodal site
S	Spleen involvement
X	Bulky disease

2.1.6. Treatment of non-Hodgkin lymphoma

Treatment of NHL usually involves the combination of radiation therapy, single agent or combination chemotherapy, immunotherapy, or radioimmunoconjugate therapy. Surgery alone can be performed only in conditions where the lymphoma is localized. Radiotherapy alone can be used in localized lymphomas or to relieve suffering of patient from lymphomas. In children, NHL radiotherapy is not a recommended procedure, and it use is restricted only to proven NHL cases of the CNS, the head and neck isolated tumour [20]. Chemotherapy is the most common therapeutic procedure, especially, in aggressive lymphomas of diffuse large B-cell. Monoclonal and radioimmunoconjugate therapy are the standard and most commonly used treatment methods in the early stage of indolent lymphomas [32].

2.1. Diagnostic methods

In addition to the patient's history and physical examination, laboratory tests, such as, complete blood count, basic blood chemistry, liver and renal function tests, erythrocyte sedimentation rate (ESR), albumin, lactate dehydrogenase (LDH) tests are performed. Imaging methods are also used for further confirmation of diagnosis,

to determine the level of spread of the cancer in the body, staging, treatment planning, follow-up and prediction of disease prognosis [22]. The most common diagnostic and staging methods are:

2.1.1. Chest X-ray

Most NHL involvement of the thoracic cavity, such as, lymphomas of the lymph nodes, lung parenchyma, pericardium, pleura, and the chest wall, can easily be confirmed with the conventional chest x-ray [30]. From the chest x-ray image, one can get information about the involvement of NHL in the chest and mediastinum areas of the patient, fig.2.1.

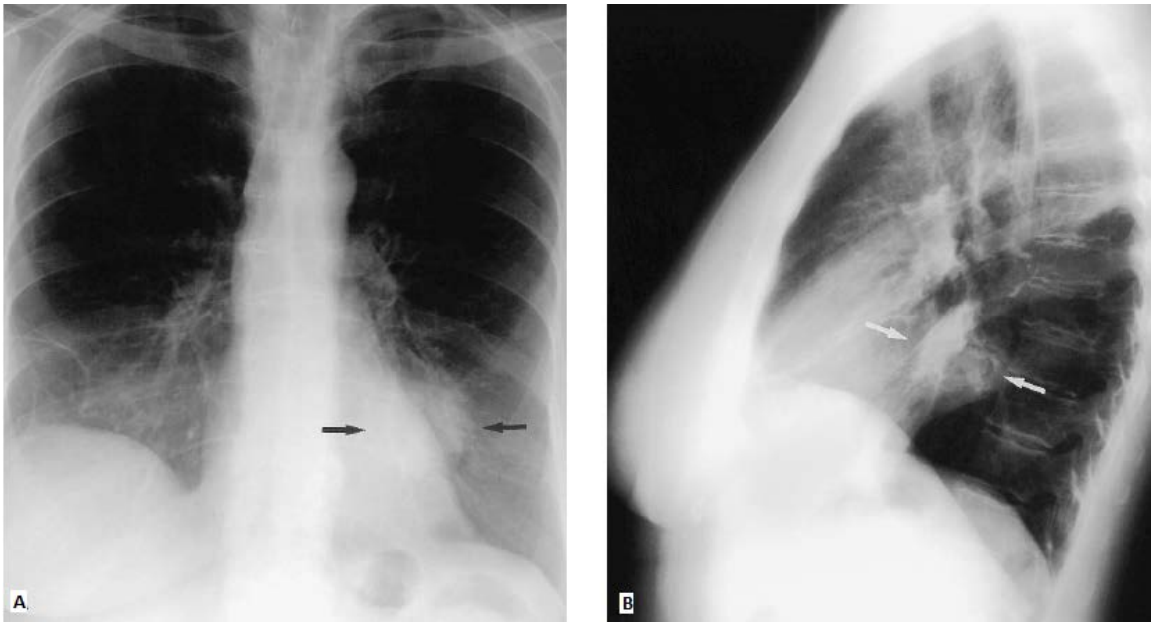

Fig.2.1 Posteroanterior (A) and lateral (B) chest radiographs in a 69-year-old female with non-Hodgkin lymphoma manifesting as an ill-defined solitary mass in the left lower lobe (arrows)[30].

Also the size of the tumor tissue on the image indicates the bulkiness of the tumor (It is bulky if the tumor mass is greater or equal to 33% of the maximum intrathoracic cavity) [20]. Even though the chest x-ray procedure is cheap and relatively simple, its diagnostic efficiency is hindered because of its lower resolution, blurring, and superimposed structures. Because of its difficulties in imaging soft tissues and exposing patients to ionizing radiation, its application to lymphoma studies is less.

2.1.2. Computed tomography scan

Computed tomography is the most common imaging modality used for diagnosis and initial staging of lymphomas [1, 33]. A CT produces a tomography image from projections of the object at multiple angles by image reconstruction. The rapid enhancement of CT technology such as: the introduction of spiral CT, which tremendously decrease the scanning time and increase effective use of the contrast agent bolus [34], the rapid advent of multidetector row CT, which increase the data acquisition and provide thinner slice thickness, more advanced image reconstruction methods, made CT to gradually be an important modality in the diagnosis and staging of the lymphomas. CT enables tissue structures to be imaged with high resolution and better contrast, which are very significant in the diagnosis and staging of the lymphomas. Some studies show that CT change the diagnostic information obtained from chest x-rays [35, 36]. Patients who are suspected of the NHL usually have CT scan, fig.2.2, of the neck, chest, abdomen and pelvis.

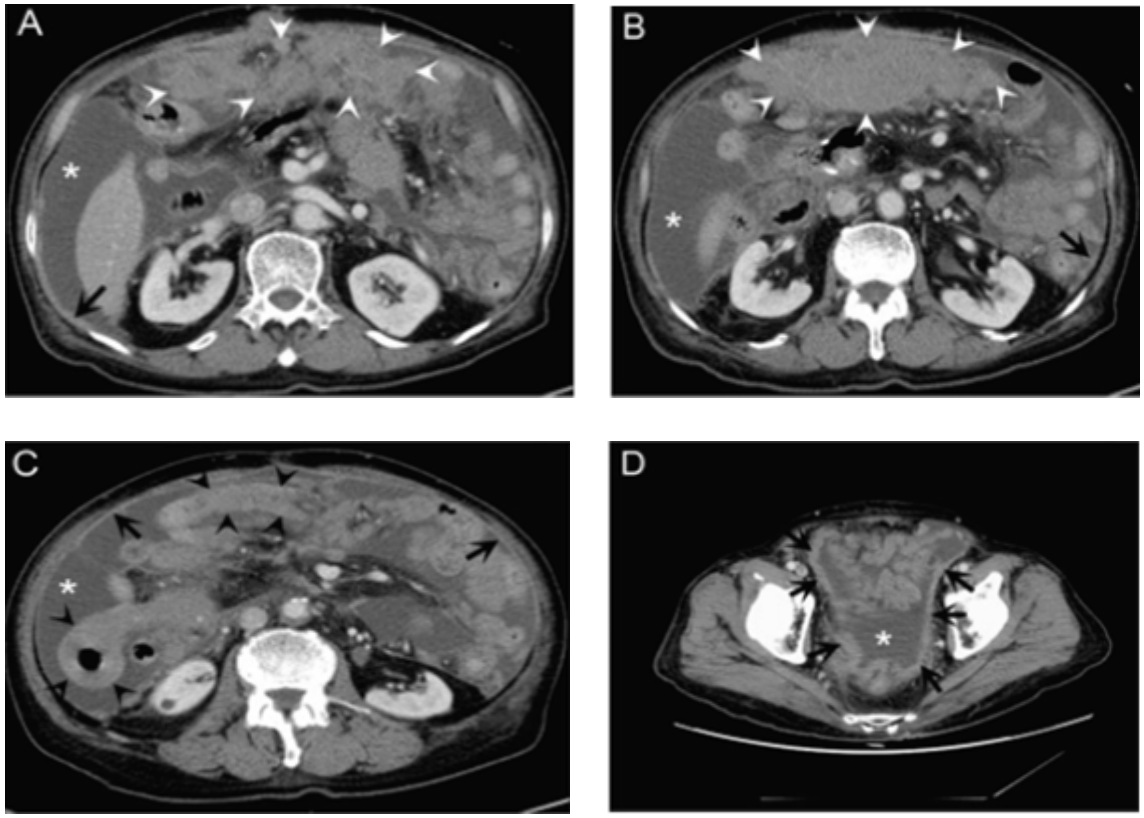

Fig.2.2. An 81-year-old man with a peritoneal lymphomatosis by diffuse large B-cell lymphoma. CT scan images (A-D) show diffuse peritoneal thickening (black arrows), diffuse nodular infiltration of omentum (white arrowheads), bowel wall thickening (black arrowheads) and ascites (asterisks) (Kim et al. BMC Cancer 2011 11:276 doi:10.1186/1471-2407-11-276).

The inherent contrast between air and bones lets CT to have a better performance in diagnosis and staging of lymphomas related to the thorax and abdomen. With the application of contrast medium, it is possible to detect small-sized extranodal lesions, which are common in NHL. CT scan acquired will give information about how many nodes are involved, the size of the tumor and the extent of the disease during diagnosis and help in the staging of NHL. The evaluation of nodal involvement by CT scan depends on the size criteria. Depending on the location of the node, various size values are used. In addition to size criteria, shape and clustering of normal-sized lymph nodes are used for diagnosis and staging purposes. Noticeable enlargement of the organ, structural change in normal-sized organ are used in the diagnosis and staging of the extranodal involvement of the lymphoma. Since nodes can be enlarged due to certain other biological processes, like inflammation or infection, plus nodes can be small sized but malignant, it is difficult for CT to distinguish such phenomena from cancerous one. Differentiation of active tumour from fibrous tissue masses after treatment is also a big challenge [37, 38, 39]. The diagnostic efficiency of CT is minimal in detecting extranodal lymphoma involvement in soft tissues, like brain, central nervous system and bone marrow. Disadvantage of CT includes the exposure to ionizing radiation.

2.1.3. Positron emission tomography (FDG-PET) scan

PET is a non-invasive diagnostic modality that uses a compound labeled with positron emitting radioisotopes as molecular probe to provide tomographic images, quantitative parameters and biochemical process of tissues inside the body. F-18 is the most common radioisotope used in the clinical application. This isotope is incorporated with different substances of biological interest, such as glucose and water. During an image acquisition, a biologically active molecule fludeoxyglucose (FDG), which is an analog to glucose, will be injected intravenously and distributed throughout the body. Normally, cancer cell do have higher glycolytic activity due to neoplastic cells. Therefore the FDG uptake by the cancer cell will be very high, fig.2.3. After a while, the positron will be emitted from the cancerous cell, combine with an electron and annihilation occurs that results in an emission of two photons which are detected at the detector to provide a tomographic image of tissue density [40].

As cancer is a biological process, its metabolic property changes with time which can be evaluated by using the FDG. This makes PET to be a widely used modality in the time course study of lymphomas. It is one of the important imaging modality used, especially, in staging and treatment follow-up of patients with NHL. An index of glucose metabolism on the PET image called the standardize uptake value (SUV), which is the ratio between the measured and expected uptake if FDG were distributed evenly throughout the body, is an important parameter used in the assessment of the degree of the lymphoma in the follow-up to treatment [16].

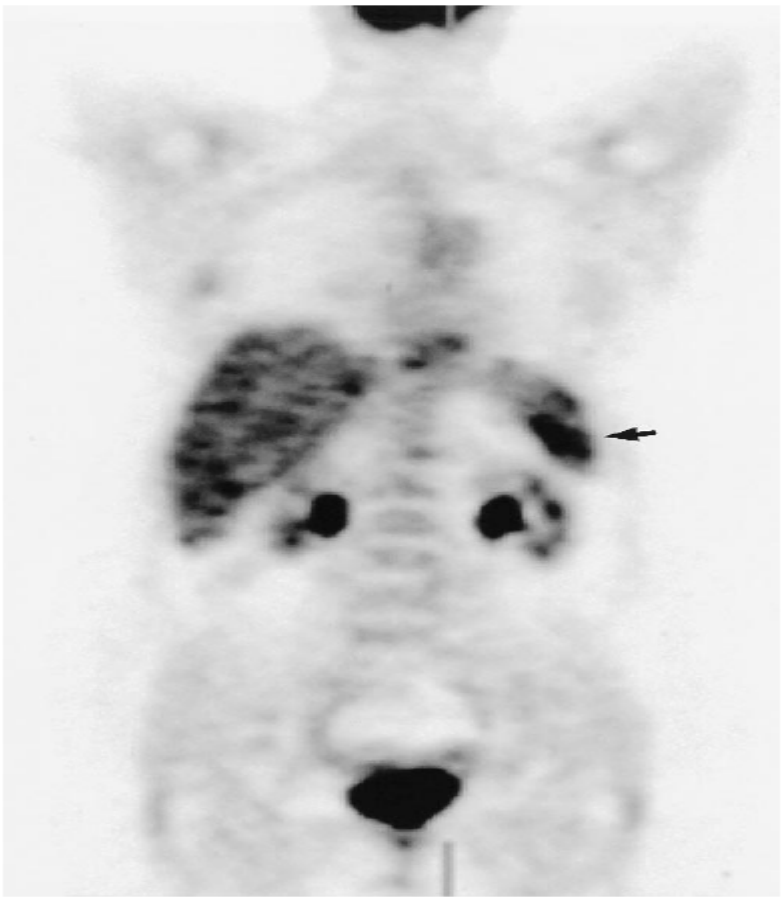

Fig.2.3. A Patient with lymphoma, referred for staging. PET images showed intense ^{18}F-FDG uptake over left sacral region [30].

Study shows that FDG-PET has a high sensitivity in the assessment of lymphoma activity in the neck and head region [41, 42]. Since detection of malignancy in PET is based on metabolic activity of the cell, it has higher performance in differentiating nodes which are enlarged due to lymphoma infiltration and that are benign. It is also reliable in the treatment follow-up process as it can distinguish active tumor from inactive ones or tissue fibrosis. Some of the limitations in FDG-PET are: exposure to ionizing radiation; having poor spatial resolution so that small metastatic nodes can be overlooked; lower uptake of the FDG may result in false negative finding; and because of the high uptake of FDG in non-tumor (benign) tissues or organ like the brain could result in a false positive PET finding [43, 44].

2.1.4. Positron emission tomography/Computed tomography (FDG-PET/CT) scan

PET/CT is relatively a recent technology which combines the functional and anatomical information provided by PET and CT respectively in a single machine, fig.2.4.

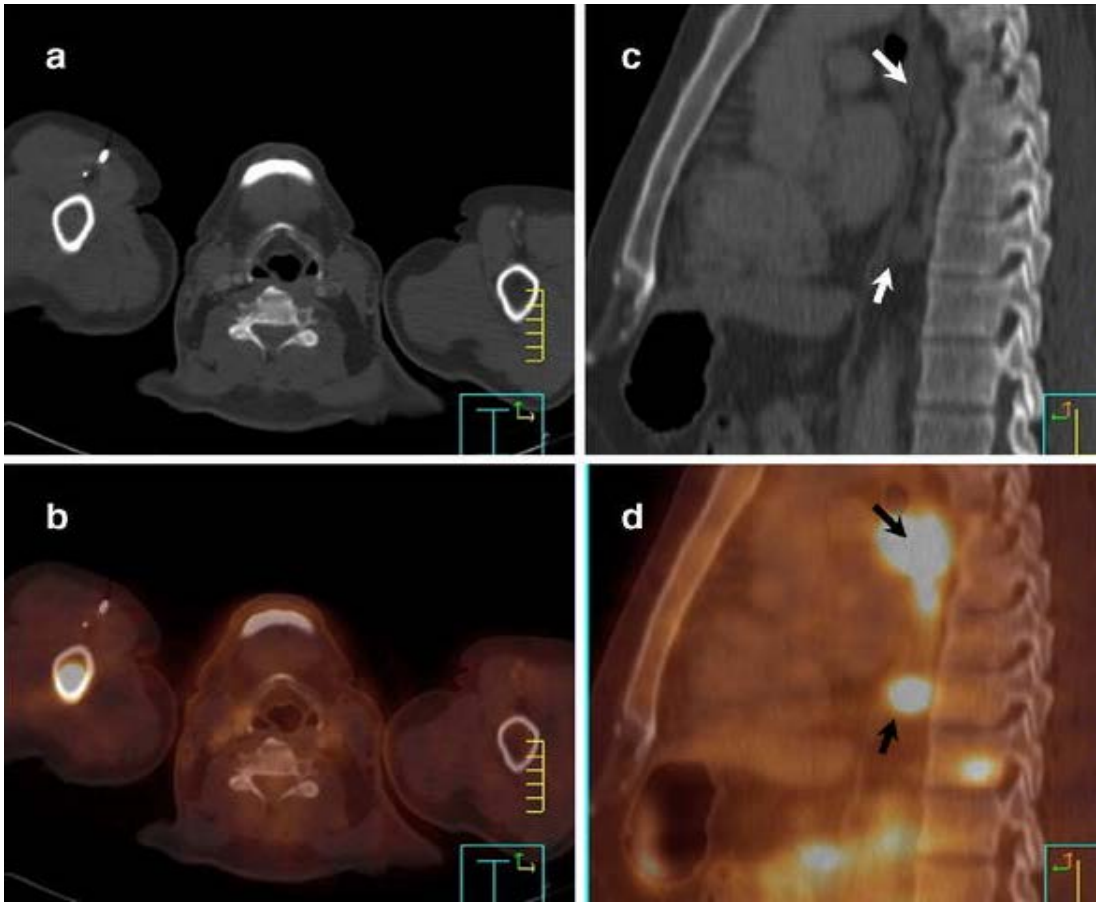

Fig.2.4 Initial staging with PET/CT in a patient with NHL Extranodal skeletal involvement of the right humerus as well as a vertebral body of the thoracic spine (biopsy proven) was not detected by CT scans (a, c), but showed pathological [^{18}F] FDG uptake on fused PET/CT images (b, d). Suspicious mediastinal lymph nodes (arrows) on CT (c) showed pathological [^{18}F] FDG uptake on fused PET/CT (d) [45].

In a single examination, PET/CT provides both metabolic- and anatomic-oriented information of a tissue under investigation. The combination of the two imaging modality outperform having CT and PET separately. Patient imaging procedure is similar to a single FDG-PET. Image analysis is based on visual and semiquantitative methods. Tissue structures with high affinity to FDG and with a matching anatomic structure from the CT are considered as abnormal. Semiquantitative parameters, like the standardize uptake value (SUV), are used to confirm the abnormality of the nodal structures. It provides important information

about small-sized lymph nodes which are false negative as per exclusive CT evaluation. Organs or tissues which have a higher glucose uptake and show increased activity on the FDG-PET image can easily be cross checked with the fused CT image and be identified as normal. In addition, benign which are not cancerous but shown to be enlarged in CT image, can be compared simultaneously with FDG-PET [46]. FDG-PET/CT has an excellent performance in the staging and follow-up of NHL involvement of the extranodal sites, such as liver, bone marrow, spleen and skin. In the assessment of treatment follow-up, tissue structures which are left as inactive after treatment can be clearly identified being not tumor by their FDG uptake [47]. Some of the limitations of PET/CT modality are: exposure to ionizing radiation, technical difficulties come up as two advanced method operate as one, one working principle may interfere with the other such as the application of intravenous contrast medium for the CT scan might create artifacts on the PET images, misregistration of PET and CT image due to breathing artifacts, and the cost for routine clinical application [14, 48].

2.1.5. Magnetic resonance imaging (MRI)

Magnetic resonance imaging (MRI) has already been a very important imaging method in diagnostic and research areas of medicine because of its potential to give an excellent soft tissue contrast way better than other imaging modalities in the absence of any radiation exposure. Moreover, the different kinds of MRI techniques available not only provide an image which tells us about the tissue density but also give information about properties of the physiochemical environment, flow and perfusion of biochemical substances inside the target tissue [49, 50, 51].

The main concept behind MRI imaging is the interaction between an external magnetic field B_0 and magnetic moment μ of spinning hydrogen protons which results in the precession of proton spins around the B_0 axis. The rate at which the proton rotate around the axis of the external magnetic field is given by the equation called Larmor equation:

$$\omega_0 \equiv \gamma \times B_0$$

Where, γ is the gyromagnetic ratio and ω_0 is the angular frequency of the proton.

The application of an external magnetic field B_0 result in the alignment of the proton in two possible orientations, with or against the direction of B_0 which result in a net magnetization vector of M in the direction of B_0. If an external radio frequency signal, RF pulse, with the same frequency as ω_0 and with a magnetic field of B perpendicular with B_0 is applied to the precessing proton, the spins absorb energy from the external RF pulse that result in the tilting of the magnetization

vector M by certain angle α, it starts to rotate in the x-y plane which results in a net transverse magnetization vector of M_{xy}. An RF pulse of 90^0 with a proper amplitude and duration, flip the longitudinal magnetization vector M_z to transverse plane with 90^0 rotations leaving no net magnetization along the B_0 axis. Once the RF pulse is off, the spins continue to rotate with larmor frequency and thus producing an RF signal which can induce a current in a receiver coil. The voltage recorded at the receiver is known as MR signal. The measured signal at the receiver coil gradually decays as the proton spins dephase or lose their synchronization. This is called free induction decay (FID). The proton spin return to their lowest energy state through two major important relaxation processes: spin–lattice (T_1 relaxation), which results in the recovery of the M_z, and spin–spin (T_2 relaxation), which results in the decay of M_{xy}. In addition to the spin-spin interaction, the external magnetic inhomogeneities contribute to the dephasing of the spin. T^*_2 is the rate of decay of the transverse magnetization because of the field inhomogeneities. The relaxation times T_1 and T_2 are inherent property of a tissue and are the base for image contrast in MRI. Each tissue in the human body has different T_1 and T_2 values; for example, fat has a shorter T_1 (recover faster) and a shorter T_2 (it decays faster) while water has a longer T_1 and T_2. By choosing an appropriate pulse repetition times (TR) and echo times (TE), it is possible to change the weights of T_1 and T_2 in the received signal so as to change the contrast between tissues. Selection of the slice and encoding of the spatial information in each slice is performed by the gradient coils of the MRI. The gradient coil generates time and distance varying magnetic fields which is used for the localization of signal from the target. Depending on the axis of image acquisition, x- , y- and z-axis gradients are used for section selection, phase and frequency encoding. Once the MR system have the information about amplitude and spatial location of the signal of the target, it will store it to the K-space, a matrix of voxels where the information about the frequency and phase of each spin is stored in the MR imaging system and Fourier transformed to get the final MR image [49, 50, 52, 53].

To obtain different kinds of MR images, different combination of RF pulses and gradient fields are used. These sequences are called imaging sequence. As the dephasing of the spin occurs instantly after the removal of the RF pulse, without the proper imaging sequence, it is difficult to get sufficient signal to produce MR image. Pulse sequences are used to rephase the spins, decrease the inhomogeneity of the external field, control the TR and TE values and thereby generate an echo signal. A180^0 RF pulse and gradient are the two mechanisms used to rephase spin in MR system. By using these two mechanisms, the two most important and basic sequences called the spin echo (SE) sequence, which uses 180^0 RF pulse, and the gradient echo (GRE) sequence, which uses gradient, are used for producing different MR images.

Conventional SE sequences are usually very long while fast or turbo SE (FSE/TSE) is used to reduce the image acquisition time in MRI. In a FSE sequence,

instead of using a 180^0 RF pulse to produce one spin echo, a train of 180^0 RF pulses are used after a 90^0 RF pulse to produce an echo and thereby decrease the number of excitation needed and scanning time. The reduction on acquisition time is inversely proportional to echo train length (ETL) or turbo factor, which is the number of 180^0 RF pulses and resultant echoes.

In a GRE sequence, as opposed to 180^0 RF pulses, an RF pulse which partially tilt the magnetization vector into the transverse plane is used. A bipolar readout gradient is used to dephase and rephase the transverse magnetization and thereby producing an echo called gradient echo. Even though gradient rephasing is not as efficient as RF rephasing, it is faster and has shorter scan time. GRE sequence is sensitive to field inhomogeneities and T_2^* weighted image are mainly dealt with a long TE values [50-53]. Gradient sequences can be coherent (refocused) or incoherent (spoiled). Both sequences implement a very short TR that is shorter than the relaxation time, T_1 and T_2, of the tissue, and because of this, there will always be a leftover transverse magnetization on the successive TRs, and the transverse magnetization will remain on a steady state. Thus only T_2* dephasing occurs in the tissue. The coherent GRE sequence uses a rephasing gradient which rephase the dephasing transverse magnetization. This result in the build-up of residual transverse magnetization and T_2* effect. Thus tissues which have long T_2 relaxation time, such as, CSF, will show higher signal intensity in this sequence. Whereas in spoiled GRE sequence, a spoiler gradient or RF pulse is used to dephase any residual transverse magnetization, and this results in contrast of T_1 weighting. Thus the spoiled GRE sequence is used for generating T_1W MR images. This sequence uses a very short TR so as to decrease the total image acquisition time and is implemented clinically in conditions where a fast image acquisition, such as, whole body imaging, dynamic contrast enhanced MR imaging, breath-hold imaging, such as in volumetric interpolated breath-hold examination (VIBE), and 3D image acquisition are needed [53-56].

Due to the superior localization of soft tissues, MRI is found to be excellent in diagnosing lymphoma involvement of brain, spinal cord and bone marrows. Clinically, there is no as such accepted golden standard MRI imaging technique. Depending on the anatomy of body part, the disease type being dealt, the advancement of the MRI on use, and the radiologist experience, different radiologists prefer different MRI sequences. Despite this, fat-suppressed, T_1-weighted gradient echo sequences before and after the administration of intravenous contrast medium and fat-suppressed T_2-weighted short tau-inversion-recovery (STIR) sequence are the most commonly practiced MRI sequences [33].

The T_1 and T_2-weighted MR imaging with and without contrast agent are the most commonly used techniques that are performed in various lymphoma studies. Most cancerous tissues have high water content than normal tissues which results in

the longer T_2 relaxation time and higher signal intensity (brightness) on the MRI image. Lower signal intensity on T_1-weighted image and higher signal intensity on T_2-weighted image are the bases for diagnosis of lymphomas on MRI images.

About 25% to 40% of patients with NHL are expected to have infiltration of the bone marrow. Hence, identification of bone marrow involvements of NHL is very important for appropriate treatment planning and disease prognosis. Bone marrow biopsy, which is an invasive and risky procedure, is still considered as a golden standard in the diagnosis of lymphoma involvement of bone marrow. When the bone marrow infiltration is localized in small area of tissues, bone marrow biopsy procedure, such as iliac crest biopsy, could lead to false-negative results. While MRI, especially, whole body MRI, provides the assessment of the large areas of the bone, and if combined, it can enhance the diagnostic efficiency of bone marrow biopsy. Conventional T_1-weighted, short TR, short TE, spin-echo technique (T_1-SE), conventional T_2-weighted, long TR, long TE, spin-echo technique (T_2-SE), and STIR technique are used for detection of lymphoma in the bone marrow [57,58].

On T_1-SE MRI sequence, the short T_1 relaxation time of the fat, due to an efficient spin-lattice interaction of proton spin in the bone marrow, results in high signal intensity on the MR image while the tumour have longer T_1 relaxation time; due to the inefficient spin-lattice interaction of proton spins of the tumour; that generate a dark signal intensity on the MR image. On the T_1-SE MR image, red marrow of the bone, which consists of almost half percent of water, appears darker than fatty marrow, and this may result in difficulty of detection of the tumour. On T_2-SE MRI sequence, the fat appears to be dark because of the shorter relaxation time T_2 while the water rich tumour will appear bright as it has a long relaxation time. On T_2-SE MRI sequence, the presence of necrosis or inflammatory debris which shows tumour activity and appears as bright on MR image makes distinguishing of the malignancy difficult [57-60].

STIR is a contrast generating MRI sequence that is used to suppress the high signal intensity from fat so that the signal from tumour tissue is enhanced. In STIR spin echo sequence, 180^0 RF pulse is applied to flip the magnetization vector from fat tissue by 180^0. Once the RF pulse is removed, the spin from fat and surrounding tissues start to relax and as the net magnetization vector cross the transverse plane at a time τ where the net magnetization for fat becomes zero, the application of a 90^0 RF pulse will flip the net magnetization from other tissues. The transverse magnetization from other tissues will induce a signal in the coil, but as there is very little or no transverse magnetization for fat tissue, signal will not be detected by the receiver coil, and this results in dark MR image of fat. Additive T_1 and T_2 are shown in the STIR MR image, and tissues with long T_1 and T_2 value, like water, will have higher intensity (brightness) on the MR image. With STIR imaging sequence, the high water containing tumour will have high signal intensity with the fat suppressed dark background MR image. The STIR sequence is found to be superior in detecting lymphoma of the bone marrow than the T_1-SE sequence, and STIR also have the

potential to differentiate marrow sclerosis from tumours since marrow sclerosis appear dark and tumour appear bright on STIR sequence while both marrow sclerosis and tumour appear dark on T_1-SE sequence [57-61].

The combined MRI sequence, STIR and T_1-SE, is found to be a sequence which gives better image quality for the study of the involvement of lymphoma with bone marrow. Recently, the conventional T_2-SE and STIR MRI sequence are being replaced by the fast spin echo (FSE) sequences, T_2-FSE and FSE STIR MRI sequences respectively. By implementing the FSE sequences, it is possibly to get as good quality as conventional SE sequences with much shorter time. The fat suppression MRI sequences expand the dynamic range of the image display by suppressing the high signal intensity from fat so as to improve tissue contrast [62-66].

Contrast enhanced (CE) MRI technique is a method used to enhance the visibility of targeted tissue. Contrast enhancing material, such as, Gadolinium-DTPA, increases the T_1 relaxation of the target tissue, in such case, the malignant tissues, so that non-malignant tissues which are isointense with the malignant on the MR image can be discriminated. Infiltration of bone marrow by lymphoma is better visualized using contrast enhanced T_1-weighted MR than T_1-weighted MR sequence. In the post treatment evaluation of patients with lymphoma, the enhanced T_1 MRI can help in differentiating active lymphoma from non-active lymphoma [61, 67]. CE-MRI is a method of choice in the study of lymphoma involvement of the central nervous system (CNS). NHL is the most common form of CNS lymphomas. In the study of lymphoma involvement in the CNS, MRI sequences of T_1-weighted SE, T_2-weighted FSE, contrast enhance T_1-weighted and fluid-attenuated inversion-recovery (FLAIR) are mainly used. Because of the high nuclear-to-cytoplasmic ratio and dense cellularity of the tumours in the primary CNS lymphoma, it is used in differentiating it from other brain malignancies since most of the brain tumors have longer T_2-relaxation and higher signal intensity on MR image due to high water content of the tumor. Studies of lymphoma involvement of CNS show the use of contrast agent to the conventional spin echo technique will completely enhance the diagnostic efficiency of the MRI. Lesions, which are small and located very close to the CSF, are difficult to be detected by T_2-weighted MR sequences due to the higher signal intensity from the CSF which may obscure the lesions. This can happen especially at the early stage of disease, when the lesion is small. FLAIR is a SE-based MRI technique which is used to create image contrast by nulling the signal from CSF. The principle is the same as the STIR sequence which is used for suppressing signals from fat. Eliminating the signal from CSF helps in delineating lymphomas of small size, located adjacent to CSF with hyperintense signal on MR image. The ability of FLAIR in detecting small-sized lesion at early stage is crucial and contributes to the staging, treatment planning and also improves the prognosis of the patient [68-73].

Enlargement of mediastinal lymph nodes, parenchymal anomaly, and pericardial, pleural, and chest wall involvement of the lymphoma, called thoracic lymphoma, are frequently studied before and after contrast material methods using T_2-weighted FSE and T_1-weighted SE (T_1W-SE). On T_1W-SE, enlarged lymph nodes will appear as hypointense to fat, and they appear as hyperintense or isointense to fat on T_2W-SE [74]. In the treatment follow-up of patients with mediastinal lymphoma, tissues which show high signal intensity with a homogenous pattern on a T_2W image corresponds to be an active tumour while the same tissue appears in a homogenous low intensity pattern on a T_1W MR image. A mixed pattern of high and low signal intensity on the T_2W images often corresponds to a mixture of active tumour and some other tissues, such as, fibrosis, and inflammation that often appear after early treatment. A homogenous pattern of hypointense intensity on T_2W images is characteristic of inactive fibrous tissue. Tissues which show high homogenous enhancement on T_1W after contrast are assumed to be active tumour while those tissues which show mixed enhancement correspond to the presence of mixed tissue, active tumour and inactive fibrosis, or inflammation whereas tissues with no or low enhancement correspond to the inactive fibrosis. MRI has a better diagnostic efficiency in the treatment follow-up if it is used after 6 months of treatment [75, 76, 77].

The evaluation of thoracic lymphoma using MRI is liable to artifact that arises due to the movement of the thoracic and abdominal region while breathing which results in blurring and loss of image resolution. In order to maintain the quality of the output image, various MRI techniques are clinically implemented. In the simplest imaging technique called breath-hold imaging, the patient will hold his/her breath for a short period of time which is efficient in reducing the artifact. For this technique we need a fast image acquisition technique as conventional spin echo (CSE) is not fast enough for this purpose. A fast imaging technique such as Turbo SE, HAST (half-Fourier single-shot turbo spin echo) techniques are used. HAST is similar to TSE sequences with a single-shot RF pulse. In this sequence, after a single RF excitation, a bit more than half of the k-space will be acquired and the rest will be filled by mirror symmetry of the k-space. Fourier transformation of the k-space will provide us the HAST MR image. Because of its higher speed, HAST imaging technique is used for breath-holding MR studies [78, 79]. In addition, volumetric breath-hold examination (VIBE) is a new gradient-echo method that uses the spoiled GRE sequence and provides a short image acquisition time which can be used for imaging of abdominal regions so as to remove movement-associated artefacts of the MR image [56].

Lymphomas are a kind of disease that can infiltrate throughout the body. Almost 40% of skeletal metastases involve the appendicular skeleton which needs an imaging method that covers anatomy of the whole body. MRI has proven to be superior in diagnosing bone and bone marrow involvement of malignancy [80, 81]. Rapid advancements in hardware of scanner (multi-receiver channel scanner),

surface coils (multiple phased-array coil), and the development of various new imaging sequence and acquisition methods (parallel image acquisition technique, PI), have made the whole body MRI (WB-MRI) technique as an alternative to multimodal imaging methods and be applied in routine clinical studies of malignant lymphoma within a reasonable scan time. As lymphoma involvement of the bone marrow is common in NHL, the role of WB-MRI in the staging process is indisputable. Even if there is no standard sequence with a considerable minimal time for WB-MRI method, the STIR sequence is found to be more sensitive [82, 83]. Depending on the anatomical location to be imaged, different MRI protocols can be used. In dedicated MRI, T_1-weighted SE and STIR imaging sequence are found to be important in the assessment of lymphomas of the bone marrow and lymph nodes [84, 85, 86]. Hence, in WB-MRI lymphoma studies, coronal T_1-weighted FSE and coronal STIR imaging sequences are used in the assessment of the head/neck, thorax, abdomen/pelvis and lower extremity regions of the body. In order to reduce the motion artefact in the thorax and abdomen region, fast and breath-hold imaging sequences, such as, T_1-FSE, HAST, and VIBE are implemented. Since coronal MR image cannot provide all the necessary information, additional axial oriented image of the head/neck, thorax, and abdomen/pelvis regions will be taken. In addition, contrast enhanced (CE) axial T_1-FSE image of the head/neck, CE axial STIR image of the thorax, CE sagittal STIR image of the spin, and CE STIR or T_1-FSE image of the abdomen region will complement the diagnosis process [82, 87].

Most of the imaging methods that are used clinically in diagnosis, staging, and treatment follow-up of patients with nodal lymphoma mainly rely on morphological appearances, such as, size, border, and shape of the nodes in the image. But it is also true that even small-sized lymph nodes can be infiltrated by cancerous cells and lymph nodes can become enlarged with some other biological process like inflammation, and thus even after treatment, the size criteria could lead to a false analysis. Even conventional MRI analysis of lymphoma depends on the intensity of the target tissues, but in the same way, inflammation, necrosis, and cysts can show tumor activity so that the analysis still have to be based on size criteria. Studies show that this challenge can be solved with recent application of diffusion theory on MRI. Diffusion of water molecule inside tissues is affected by the normal cellular interaction within the tissues. Nodes that are involved with malignant lymphoma will have higher cellular structure which restricts the intra- and extracellular movement of water molecule in the cellular environment [88, 89, 90]. Diffusion-weighted imaging (DWI-MRI) is a technique which can isolate areas with restricted diffusion (slow diffusion of proton), lymphomatous tissue, from unrestricted (rapid diffusion of protons). Fast imaging sequences, such as, echo-planner or fast GRE sequences and two equal gradient pulses are mainly used in DW-MRI. Echo planner imaging (EPI) is a very fast imaging sequence which uses a single echo train to fill all lines of the k-space. The mechanism of producing a diffusion-weighted image is

that before image acquisition, a dephasing and rephasing gradient are applied, and if the spin that are in phase are dephased by the dephasing gradient, the signal intensity will decrease, and if the same but opposite gradient is applied, the spin will be rephrased again, and this results in high signal intensity on MR image. This happens in a condition where there is restricted motion of protons between the times of the applied gradients, which is in cancerous tissues. Whereas, in normal tissues, spin motion is not restricted and spin undergoes phase shift which results in decrease of intensity on the MR image [50, 55, 91, 92, 93]. The presence of high intensity on the DWI-MR image could be from the longer T_2 effect (normal tissues having longer T_2 decay time), the phenomenon called T_2 shine-through, which can cause wrong diagnosis. Apparent diffusion coefficient (ADC) mapping is a technique that is derived from ADC maps. An ADC map is calculated mathematically by comparing images obtained with DW against without DW. In an ADC map, areas of restricted diffusion (cancerous tissue) appears as dark whereas normal tissues appear bright [55], for example, DLBCL, the most common form of NHL, shows high signal intensity in DWI and low signal in ADC mapping. The ADC value is not dependent of the magnetic field strength and can remove the T_2 shine-through effect. Hence to confirm the diagnosis of diffusion restriction, comparing DWI against ADC mapping is important [14]. Studies show that the challenge in differentiating between the benign and malignant lymphadenopathies can be solved by DWI incorporated with ADC mapping [88, 89, 91, 93]. DWI with ADC mapping can be used in treatment follow-up of patients with lymphoma. Study shows that DWI with ADC mapping is capable of providing comparable diagnostic results as the PET/CT imaging method [14].

2.1.6. Biopsy

It is a procedure where a piece of tissue is taken from the cancer suspected part of the body and examined, usually, under microscope. A pathologist will examine the tumor tissue under microscope and study the features of the cells in the surrounding tissue and examine in detail the antigens on the surface of the cells [22, 31, 94]. Biopsy is an important procedure to confirm the type, histopathology and confirmation of the diagnostic results of other procedures of lymphoma. The most common biopsies are:

Excisional or incisional biopsy: A biopsy where a surgical removal of the entire node is performed (e*xcisional biopsy*) or small part of the tumor is removed (*incisional biopsy*) for further examination. It is a preferred biopsy procedure because it preserves the architecture of the node and gives a relatively large sample for examination [22, 31, 94].

Needle biopsy: In a condition where the suspected tissue is deep inside the body, a fine needle is inserted into the tissue, called fine needle aspirate (FNA) and sample

is removed for examination. A larger tissue can be taken by a bore needle called core needle biopsy. For deeper tissues, an image (CT or ultrasound) guided biopsy is performed. FNA is usually performed to study for patients already diagnosed of lymphoma or in the disease relapse [22, 31, 94].

Bone marrow aspirates and biopsy: They are performed to check whether there is bone marrow involvement of the lymphoma or not. As bone marrow involvement by NHL is frequent, it is highly recommended for NHL patients [22, 31, 94].

2.2. Image analysis method

The fast evolving technology of MRI makes it promising for better diagnosis, treatment, and follow-up of patients. Clinically, once images are acquired, qualitative, quantitative, or both, image analyses are used in the disease diagnosis process and in the evaluation of information content of the image.

2.2.1. Qualitative MRI image analysis

In a clinical environment, diagnosis and evaluation of diseases from MRI image are usually based on qualitative image analysis methods. Qualitative image analyses are subjective, experience-based, and are usually based on visual assessment of the acquired image for an abnormal feature in the image such as morphological appearances, including size, border and shape of the tissues or nodes on the acquired images. A lot of research has been done to compare the different MRI sequences for different disease diagnoses or evaluation of responses to treatment. Many have used qualitative method to compare the different sequences. Visually comparing the sequences and giving rank have been used in a lot of studies.

2.2.2. Quantitative MRI image analysis

Quantitative image analyses involve different techniques, such as, texture analysis of image to extract certain features and parameters, and curve fitting between image sets acquired at different time points to extract quantitative information, such as, water content or relaxation time. Quantitative image analyses are more reliable and less prone to intra- and inter-observer variability, but are usually implemented on research level [95].

Contrast values collected from different MRI sequences are important quantitative parameters for comparing MRI sequences. In addition to morphology, contrast plays a vital role in the disease diagnoses, staging and follow-up of lymphoma patients. The relaxation times in MRI are inherent property of a tissue and are the bases for image contrast. Each tissue in the human body has different T_1 and T_2 relaxation values and hence different intensity on different sequences. Thus

the conspicuity of tissue can be varied by using different MRI sequences. Upon visual analysis, the sequence which depicts the target tissue with higher contrast or makes the target tissue distinguishable from other surrounding tissue is used in the diagnosing process.

The contrast level of a target tissue can be defined in different ways. In this study the Weber contrast,

$$C = \frac{S_a - S_b}{S_b} \qquad (1)$$

is used, where S_a and S_b are the signal intensities of the target and the reference , surrounding or adjacent tissue.

Thus contrast, a simple quantitative parameter, is measured from MRI images and is less prone to intra- and inter-observer variability.

Once the contrast ratio is calculated for the different MRI sequences, the data can be analyzed using different statistical techniques. Depending on the data, parametric or non-parametric statistical methods are used. The parametric method usually assumes that the data is drawn from a normally distributed population whereas the nonparametric make no assumption about the population where the sample is drawn from. Nonparametric statistical methods are preferred when the data is not normally distributed or in a condition when the numbers of data are small. Wilcoxon Signed Rank Test is a nonparametric statistical method that is used for comparison of two paired data on repeated measurements. In this work, SPSS statistical software is used for analyses.

3. MATERIAL AND METHODS

3.1. Patient

In this study MRI images of eighteen patients (thirteen men and five women; mean age, 62 years) with aggressive DLBC NHL are used. Patients were part of a big research project work on aggressive lymphoma study. The inclusion and exclusion criteria are briefly described in reference 14. The study is approved by the Ethics Committee of Tampere University Hospital.

All patients had physical examination, standard laboratory tests for lymphomas. In addition, unilateral bone marrow aspiration and trephine biopsy were performed on each patient. Pathological samples were reviewed by expert hematopathologists and classified according to the WHO/Revised European–American Lymphoma classification of lymphoid neoplasm [14].

All but patient three, ten and eighteen were imaged by MRI before enrolment to treatment (E1) and one week after the first dose of chemotherapy (E2). Patient three, eleven and fifteen underwent only MRI scanning before treatment (E1). In addition patient ten had no T_2W fat suppression MR sequence.

3.2. MRI acquisition

MRI image was acquired using a 3-T MR System (Siemens Trio-Tim, Erlangen, Germany) with the manufacturer's body and spine array coils. The body matrix coil had six elements and dimensions of 322 mm ×520 mm ×40 mm (L × W × H). The body matrix coil was used in combination with the spine matrix coil that had 24 elements and dimensions of 185 mm× 485 mm× 33 mm (L × W×H). The appropriate number of spine coil elements was connected to cover the anatomy of interest. In addition, a neck coil was used for examination of the cervical region. It had four elements with a patient bore of 225 mm× 205 mm (H × W) and coil outer dimensions of 190 mm×330 mm×332 mm (L× W×H). The MRI examination consisted of whole-body screening from the level of the skull base to the floor of the pelvis in the coronal plane using a parallel acquisition technique that allows for the improvement of spatial resolution without prolonging data acquisition. Because the coronal imaging had a limited field of view to cover the whole body, the upper and lower body trunks were imaged separately in the coronal plane.

In this study MRI protocols, an axial T_1-weighted, three-dimensional, volumetric interpolated breath-hold examination with fat suppression, before and after gadolinium tetraazacyclododecanetetraacetate (0.2 ml/kg Dotarem) injection, and axial T_2-weighted TSE imaging, once with and once without fat suppression, are used. Before contrast administration, DWI was acquired using a single-shot echo-planar sequence in the axial plane with two b values (0 and 800 s/mm^2). ADC map is calculated from the DWI. In addition to the axial MR images, the coronal, sagittal, DWI, ADC map and 3D MR images of the patients are also used for the accurate localization of the lesion. Below, in figures 3.1-3.4, are examples of images of the different MRI protocols.

Fig 3.1 Abdominal region lymphoma in a 68-years old man patient: Axial T_1-weighted image showing a large tumor on the left side.

Fig 3.2 Abdominal region lymphoma in a 68-years old man patient: Axial T_1-weighted image after contrast injection showing enhanced tumor.

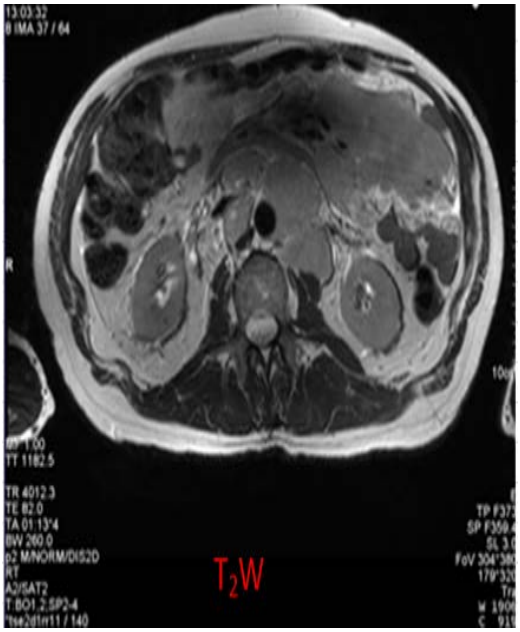

Fig 3.3 Abdominal region lymphoma in a 68-years old man patient: Axial T_2-weighted image showing a large tumor on the left side.

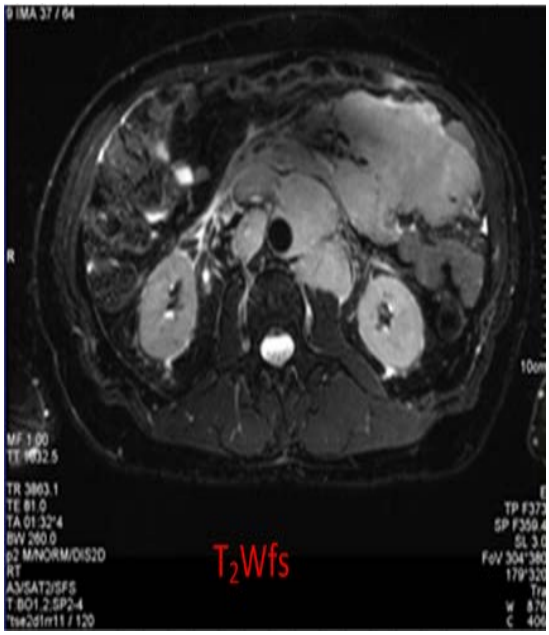

Fig 3.4 Abdominal region lymphoma in a 68-years old man patient: Axial T_2-weighted with fat suppression image showing more contrast tumor on the left side

3.3. MRI image analysis

All the MR images were viewed on a Picture Archiving and Communication System workstation. The mean signal intensity of the lesion, which is selected manually by the computer mouse, from the different MRI sequences is measured. Circular or free hand drawing is used for selection of the region of interest (ROI). Enclosing the ROI with circle or free hand drawing generates the mean signal intensity value of pixels enclosed by the ROI.

Because absolute signal intensity measurements are potentially subject to variation, dependent on the position of the ROI in relation to the surface coil and the amplifier gain of the image reconstruction circuitry, normalized lesion to normal tissue signal intensities within each MRI sequences are used. The normalized intensities are contrast ratio which conveys information about the performance of each sequence in delineating a lesion from normal tissue.

$$C = \frac{S_l - S_n}{S_n} \qquad (2)$$

Where C is the normalized contrast intensity ratio, S_l is the absolute lesion signal intensity and S_n is the absolute normal tissue signal intensity, which in this case is the vertebral tissue.

Once the target lesion is identified visually in each MRI sequence, ratios were calculated comparing the signal intensity value of target lesion with the signal intensity value of the normal tissue. Table 3.1 and table 3.2 show the absolute and normalized signal intensities of the four MRI sequences at time point E1 and E2 respectively. The normal tissue is chosen from the same slice as the lesion and as the vertebral tissue is easily detectable from different MRI sequences and its mean signal intensity value is fairly the same; it is found appropriate to make the vertebral tissue as a reference tissue against the lesion. Examples of images of MRI are shown in figures 3.5-3.8 below.

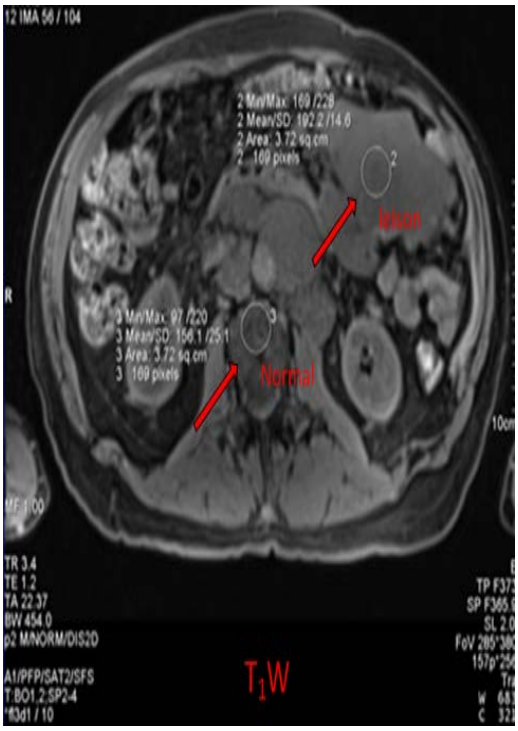

Fig 3.5 Abdominal region lymphoma in a 68-years old man patient with a region of interest in tumor and normal tissue on Axial T_1-weighted

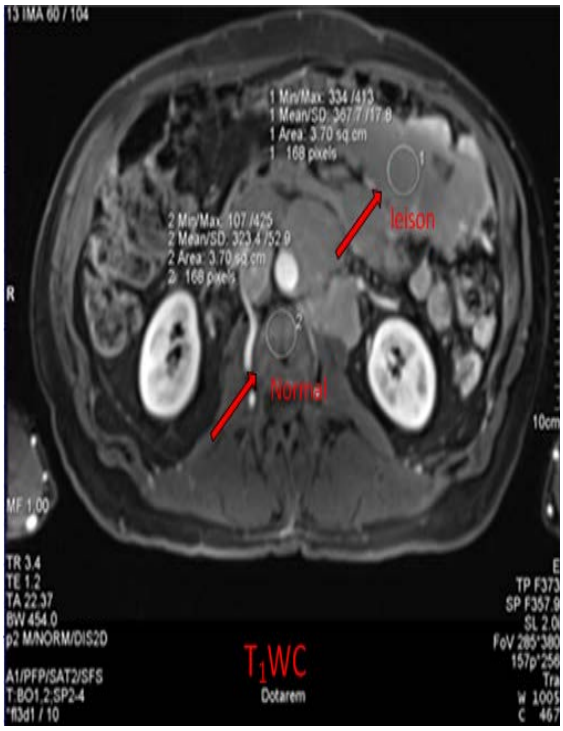

Fig 3.6 Abdominal region lymphoma in a 68-years old man patient with a region of interest in tumor and normal tissue on Axial T_1-weighted image after contrast injection.

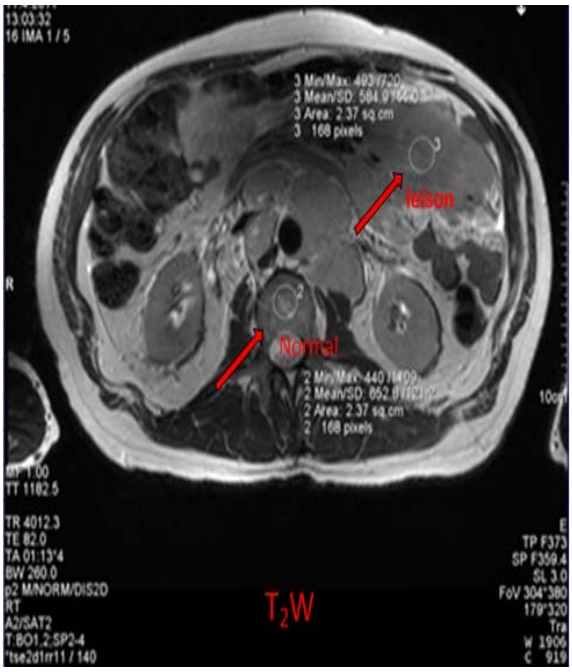

Fig 3.7 Abdominal region lymphoma in a 68-years old man patient with a region of interest in tumor and normal tissue on Axial T_2-weighted image.

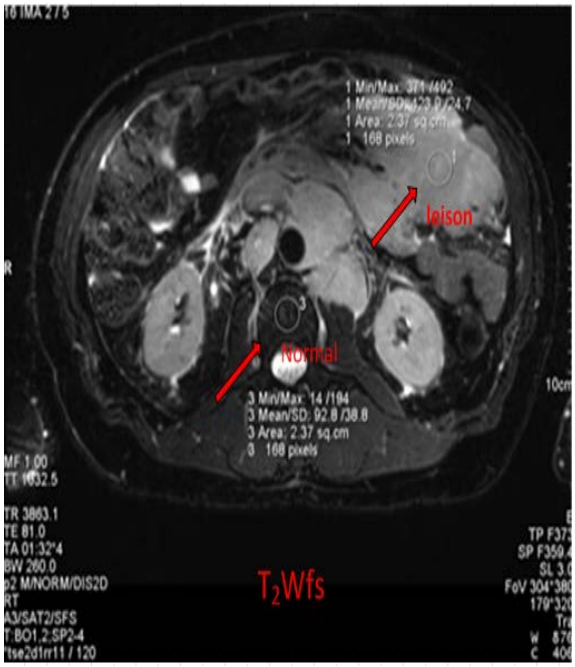

Fig 3.8 Abdominal region lymphoma in a 68-years old man patient with a region of interest in tumor and normal tissue Axial T_2-weighted with fat suppression.

Table 3.1. Absolute and normalized signal intensities of the four MRI sequences at time point E1.

Target	Sex	Age	E1T$_1$Ld	E1T$_1$Bd	E1T$_1$	E1T$_1$_cLd	E1T$_1$_cBd	E1T$_1$C	E1T$_2$Ld	E1T$_2$Bd	E1T$_2$	E1T$_2$_fsLd	E1T$_2$_fsBd	E1T$_2$fs
Abdomen	F	56	182	260	-.30	412	269	.53	435	495	-.12	337	166	1.03
Abdomen	M	61	208	137	.52	446	240	.86	389	455	-.14	398	244	.63
Neck	M	57	189	289	-.35	498	372	.34	581	290	1.00	581	166	2.50
Neck	F	51	215	321	-.33	650	458	.42	563	343	.64	426	147	1.90
Neck	M	78	155	175	-.11	297	231	.29	224	158	.42	221	59	2.75
Neck	M	56	286	332	-.14	691	527	.31	716	366	.96	593	169	2.51
Abdomen	F	54	205	216	-.05	490	537	-.09	630	568	.11	374	277	.35
Neck	F	32	216	313	-.31	410	418	-.02	754	1160	-.37	550	159	2.46
Abdomen	M	48	200	167	.20	394	301	.31	551	531	.04	445	86	4.17
Thorax	M	70	354	355	.00	666	487	.37	173	193	-.10			
Abdomen	F	74	197	177	.11	388	347	.12	586	645	-.09	482	118	3.08
Neck	M	75	249	317	-.21	600	448	.34	696	538	.29	642	145	3.43
Abdomen	M	47	182	115	.58	288	180	.60	372	347	.07	301	54	4.57
Thorax	M	66	501	533	-.06	816	782	.04	469	411	.14	347	191	.82
Abdomen	M	68	191	156	.22	369	349	.06	590	653	-.10	425	92	3.62
Thorax	M	66	210	118	.78	441	189	1.33	474	281	.69	356	59	5.03
Abdomen	M	76	137	105	.30	334	179	.87	477	562	-.15	419	71	4.90
Abdomen	M	79	245	171	.43	568	305	.86	717	469	.53	541	113	3.79

E1,time point E1;T$_1$, T$_1$ W MRI sequence; Ld, signal intensity of the lesion (Lesion density);Bd, signal intensity of the bone(vertebrae); T$_1$_C, T$_1$ W MRI sequence with contrast agent; T$_2$, T$_2$ W MRI sequence; fs, fat suppression.

E1T$_1$=E1T$_1$Ld- E1T$_1$Bd/ E1T$_1$Bd;

E1T$_1$C= E1T$_1$_cLd- E1T$_1$_cBd / E1T$_1$_cBd;

E1T$_2$= E1T$_2$Ld - E1T$_2$Bd / E1T$_2$Bd;

E1T$_2$fs= E1T$_2$_fsLd - E1T$_2$_fsBd / E1T$_2$_fsBd;

Table 3.2. Absolute and relative signal intensities of the four MRI sequences at time point E2.

Target	Sex	Age	E2T$_1$Ld	E2T$_1$Bd	E2T$_1$	E2T$_1$_CLd	E2T$_1$_CBd	E2T$_1$_C	E2T$_2$Ld	E2T$_2$Bd	E2T$_2$	E2T$_2$_fsLd	E2T$_2$_fsBd	E2T$_2$fs
Abdomen	F	56	204	167	.22	458	240	.91	461	632	-.27	332	190	.75
Neck	M	57	212	324	-.35	559	441	.27	461	399	.16	450	148	2.04
Neck	F	51	305	361	-.16	779	544	.43	559	461	.21	408	267	.53
Neck	M	78	294	257	.14	588	439	.34	501	239	1.10	508	102	3.98
Neck	M	56	478	342	.40	992	691	.44	583	279	1.09	642	337	.91
Abdomen	F	54	239	248	-.04	568	726	-.22	816	974	-.16	581	585	-.01
Neck	F	32	264	364	-.27	549	674	-.19	732	532	.38	671	247	1.72
Abdomen	M	48	222	159	.40	447	333	.34	643	516	.25	473	110	3.30
Abdomen	F	74	204	131	.56	385	311	.24	614	674	-.09	387	88	3.40
Neck	M	75	317	314	.01	730	423	.73	567	411	.38	543	188	1.89
Abdomen	M	47	240	134	.79	474	282	.68	366	450	-.19	324	154	1.10
Thorax	M	66	912	556	.64	1416	659	1.15	317	621	-.49	317	621	-.49
Abdomen	M	68	284	149	.91	448	318	.41	710	594	.20	550	119	3.62
Thorax	M	66	213	106	1.01	370	196	.89	410	323	.27	247	65	2.80
Abdomen	M	76	206	146	.41	305	210	.45	421	489	-.14	383	110	2.48

E2, time point E2 ; T_1, T_1 W MRI sequence; Ld, signal intensity of the lesion (Lesion density);Bd, signal intensity of the bone(vertebrae); T_1_C, T_1 W MRI sequence with contrast agent; T_2, T_2 W MRI sequence; fs, fat suppression.

E2T$_1$=E2T$_1$Ld- E2T$_1$Bd/ E2T$_1$Bd;

E2T$_1$C= E2T$_1$_CLd- E2T$_1$_CBd / E2T$_1$_CBd;

E2T$_2$= E2T$_2$Ld – E2T$_2$Bd / E2T$_2$Bd;

E2T$_2$fs= E2T$_2$_fsLd – E2T$_2$_fsBd / E2T$_2$_fsBd;

3.4. Statistical analysis

The normalized mean signal intensities, contrast ratio, were used to compare the sensitivity of each sequence in the detection of the lesion. To find out whether there is a significant difference between the different groups of MR imaging sequences, a nonparametric statistics test, Wilcoxon Signed Rank Test, is performed on the normalized signal intensities. Overall significance difference is determined based on the p value. If the p value is less than or equal 0.05, then there is a significant difference in the mean normalized signal intensity between the sequences. If the p value is above 0.05, then there is no significant difference between the sequences.

A significant level (p value) of less than 0.05 is considered as statistically significant. The statistical analyses were performed using SPSS software.

4. RESULTS

Normalized signal intensities calculated from MR images of the patients at E1 and E2 were statistically analyzed. As the sample data collected are small, a non-parametric statistics technique called Wilcoxon Signed Rank Test is conducted to evaluate and compare the different MRI sequence on the calculated mean normalized signal intensities at each time points, E1 and E2.

At the time point E1, all patients had gone through the four imaging protocols and one patient had not had the T_2W fat suppression MRI sequence. After treatment, E2, sixteen patients, from the eighteen patients, MRI data was used for the analyses. All the sixteen patients at E2 had all the four imaging protocols. In nine patients the target lesions were located on the abdomen region and six were on the neck and the rest three were in the thorax. All patients had DLBCL.

4.1. Comparison between sequences at time point E1

The box plot, figure 4.1, shows that the mean normalized signal intensity distribution for T_2W fat suppression technique is much higher than the rest of the sequences and T_1W with contrast follows the second. The intensity distribution for the T_1W before contrast agent and T_2W without fat suppression looks very similar. There were eighteen patients in the T_1, T_1C and T_2-weighted MRI sequences. One of the patient had no T_2fs weighted MRI sequence.

Tables 4.1 show the mean contrast ratio of the four sequences at the time point E2. It is clearly seen that the mean signal contrast ratio is much higher on the T_2W fat suppression MRI sequence.

Having established that the mean signal contrast ratio is much higher in the T_2W fat suppression MRI sequence and also in the distribution box plot, a Wilcoxon Signed Rank Test is conducted to evaluate if this difference is really significant. Table 4.2 shows the output from the Wilcoxon Signed Rank Test and it can be seen that the p value is substantially much less than the specified p value of 0.05. This implies that there is really a significant difference in the normalized signal contrast ratio between the T_2W fat suppression and the other MRI sequence. That is the conspicuity level of the lesion is much higher in the T_2W fat suppression than the other MRI sequence.

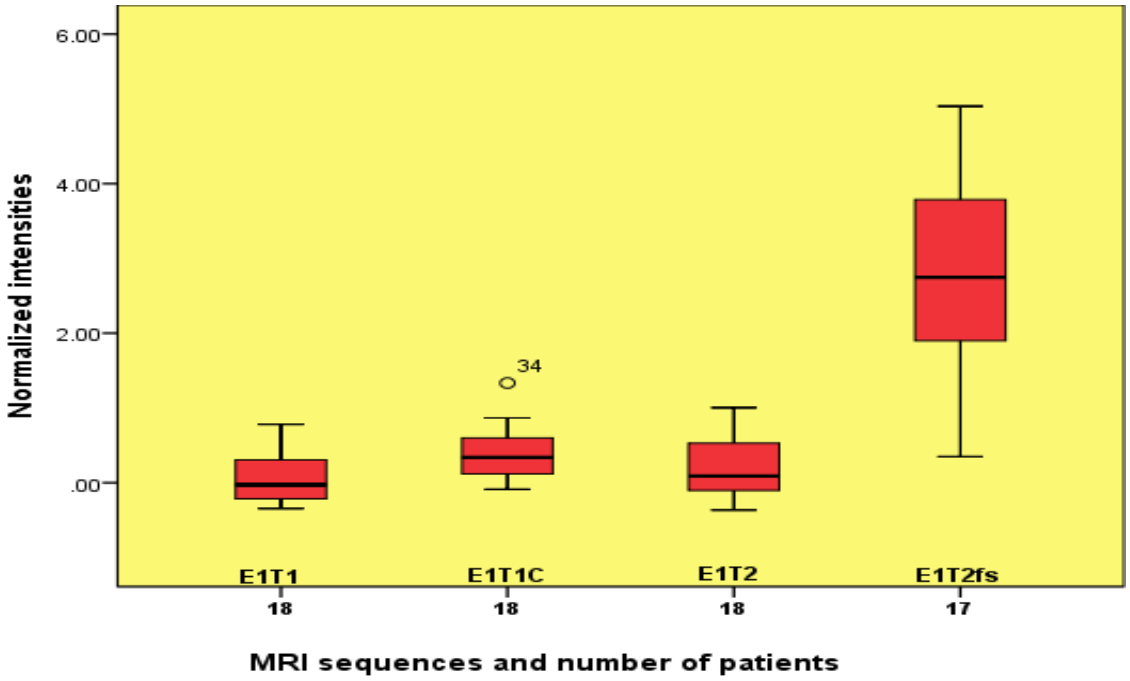

Figure 4.1. Box plot showing the distribution of the normalized mean signal intensities from the four different sequences at time point E1. T_2W fat suppression technique shows superior contrast ratio.

Table 4.1 A descriptive statistic at time point E1shows that T_2fs have the highest normalized mean signal intensity.

Descriptive Statistics

	N	Minimum	Maximum	**Mean**	Std. Deviation
$E1T_1$	18	-.35	.78	**.0714**	.34348
$E1T_1C$	18	-.09	1.33	**.4186**	.37089
$E1T_2$	18	-.37	1.00	**.2119**	.40552
$E1T_2$fs	17	.35	5.03	**2.7967**	1.48836

Table 4.2 Wilcoxon Signed Ranks Test, there is a statistically significant difference between $E1T_2fs \leftrightarrow E1T_1$, $E1T_2fs \leftrightarrow E1T_1C$, $E1T_2fs \leftrightarrow E1T_2$.

Wilcoxon Signed Ranks Test

Sequences	$E1T_2fs \leftrightarrow E1T_1$	$E1T_2fs \leftrightarrow E1T_1C$	$E1T_2fs \leftrightarrow E1T_2$
p value	**.000**	**.000**	**.000**

4.2. Comparison between sequences at time point E2

The box plot, figure 4.2, shows that the mean normalized signal intensity distribution for T_2W fat suppression technique is much higher than the rest of the sequences and T_1W with contrast follows the second. The intensity distribution for the T_1W before contrast agent is higher than T_2W without fat suppression. Fifteen patients were analyzed for the four MRI protocols.

Tables 4.3 show the mean contrast ratio of the four sequences at the time point E2. It is clearly seen from table 4.3 that the mean signal contrast ratio is much higher on the T_2W fat suppression MRI sequence.

Knowing that the mean signal contrast ratio is much higher in the T_2W fat suppression MRI sequence and also in the distribution box plot, a Wilcoxon Signed Rank Test is conducted to evaluate if this difference is really significant. Table 4.4 shows the output from the Wilcoxon Signed Rank Test and it can be seen that the p value is still substantially much less than the specified p value of 0.05. This implies that there is really a significant difference in the normalized signal contrast ratio between the T_2W fat suppression and the other MRI sequence after treatment. That is the conspicuity level of the lesion is much higher in the T_2W fat suppression than the other MRI sequence at time point E2.

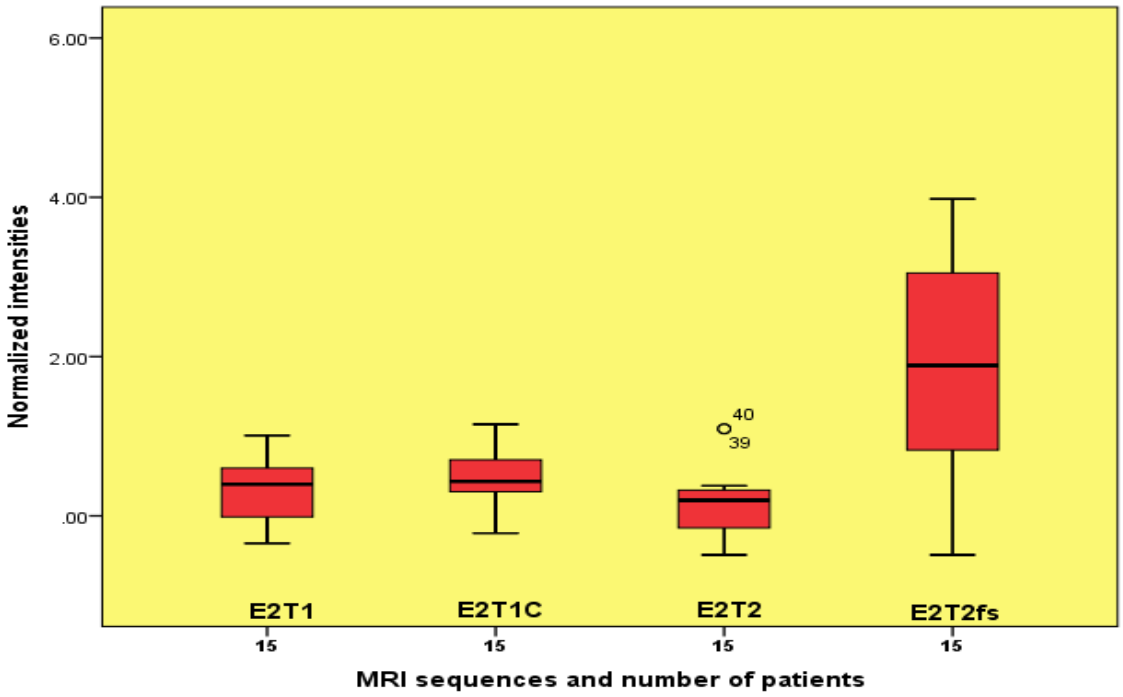

Figure 4.2. Box plot showing the distribution of the normalized mean signal intensities from the four different sequences at time point E2. T_2W fat suppression technique shows superior contrast ratio.

Table 4.3 A descriptive statistic at time point E2 shows that T_2fs have the highest normalized mean signal intensity.

Descriptive Statistics

	N	Minimum	Maximum	**Mean**	Std. Deviation
$E2T_1$	15	-.35	1.01	**.3115**	.42301
$E2T_1C$	15	-.22	1.15	**.4576**	.37533
$E2T_2$	15	-.49	1.10	**.1789**	.45011
$E2T_2fs$	15	-.49	3.98	**1.8677**	1.38519

Table 4.4 Wilcoxon Signed Ranks Test; there is a statistically significant difference between $E2T_2fs \leftrightarrow E2T_1$, $E2T_2fs \leftrightarrow E2T_1C$, and $E2T_2fs \leftrightarrow E2T_2$.

Wilcoxon Signed Ranks Test

Sequences	$E2T_2fs \leftrightarrow E2T_1$	$E2T_2fs \leftrightarrow E2T_1C$	$E2T_2fs \leftrightarrow E2T_2$
p value	**0.002**	**0.004**	**0.002**

4.3. Comparison of sequences between time point E1 and E2

Comparison between T_1W MRI sequences before contrast administration between the time point E1 and E2

The box plot, figure 4.3, shows that the mean normalized signal intensity distribution for T_1W MRI technique is much higher at the time point E2, after treatment, than at time point E1, before treatment. Eighteen patients before treatment and fifteen patients after treatment were analyzed. The mean normalized signal intensities at time point E1 and E2 can be seen from table 4.5. The mean signal intensity has shown an increment after treatment.

Once knowing that the mean signal contrast ratio is higher on the T_1W MRI sequence and also in the distribution box plot at the time point E2, a Wilcoxon Signed Rank Test is conducted to evaluate if this difference is really significant. Table 4.6 shows the output from the Wilcoxon Signed Rank Test and it can be seen that the p value is less than the specified p value of 0.05. This implies that there is really a significant difference in the normalized signal contrast ratio between the T_1W MRI sequence before and after treatment.

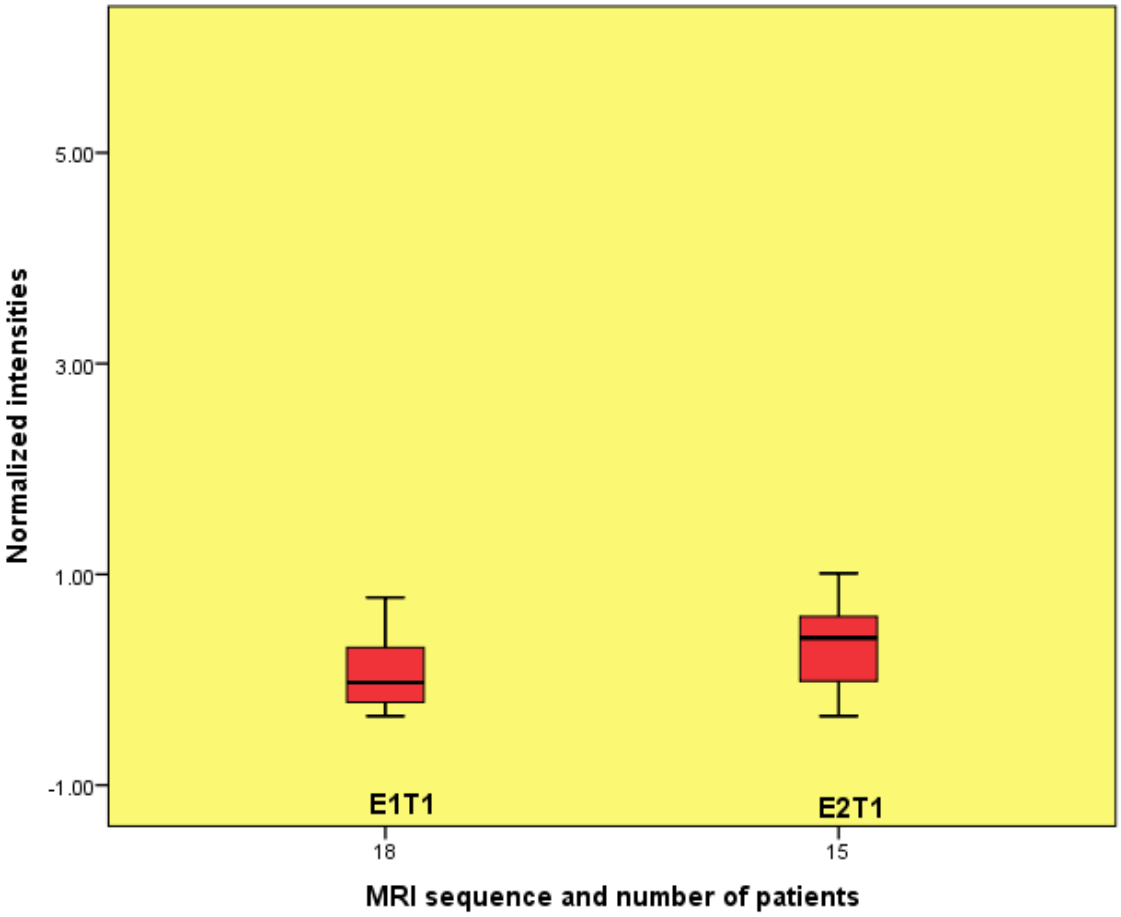

Figure 4.3. Box plot showing the distribution of the normalized mean signal intensities from the T_1w imaging sequences at time point E1 and E2. T_1W imaging technique after treatment has a higher contrast ratio than before treatment.

Table 4.5 A descriptive statistic at time point E1and E2 shows that after treatment the normalized mean signal intensity is higher than before.

Descriptive Statistics

	N	Minimum	Maximum	**Mean**	Std. Deviation
$E1T_1$	18	-.35	.78	**.0714**	.34348
$E2T_1$	15	-.35	1.01	**.3115**	.42301

Table 4.6 Wilcoxon Signed Ranks Test; there is a statistically significant difference between $E2T_1 \leftrightarrow E1T_1$.

Wilcoxon Signed Ranks Test

Sequences	$E2T_1 \leftrightarrow E1T_1$
p value	**0.001**

Comparison between T_1W MRI sequences after contrast administration between the time point E1 and E2

The box plot, figure 4.4, shows that the mean normalized signal intensity distribution for T_1WC MRI technique is a bit higher at the time point E2, after treatment, than at time point E1,before treatment. Eighteen patients before treatment and fifteen patients after treatment were analyzed. The mean normalized signal intensities at time point E1 and E2 can be seen from table 4.7. The mean signal intensity has shown a small increment after treatment.

Even if the mean signal intensity distribution on the box plot and in the table 4.7 has shown a bit increment, this increment was not significant ($p > 0.05$) as seen in the table 4.8.

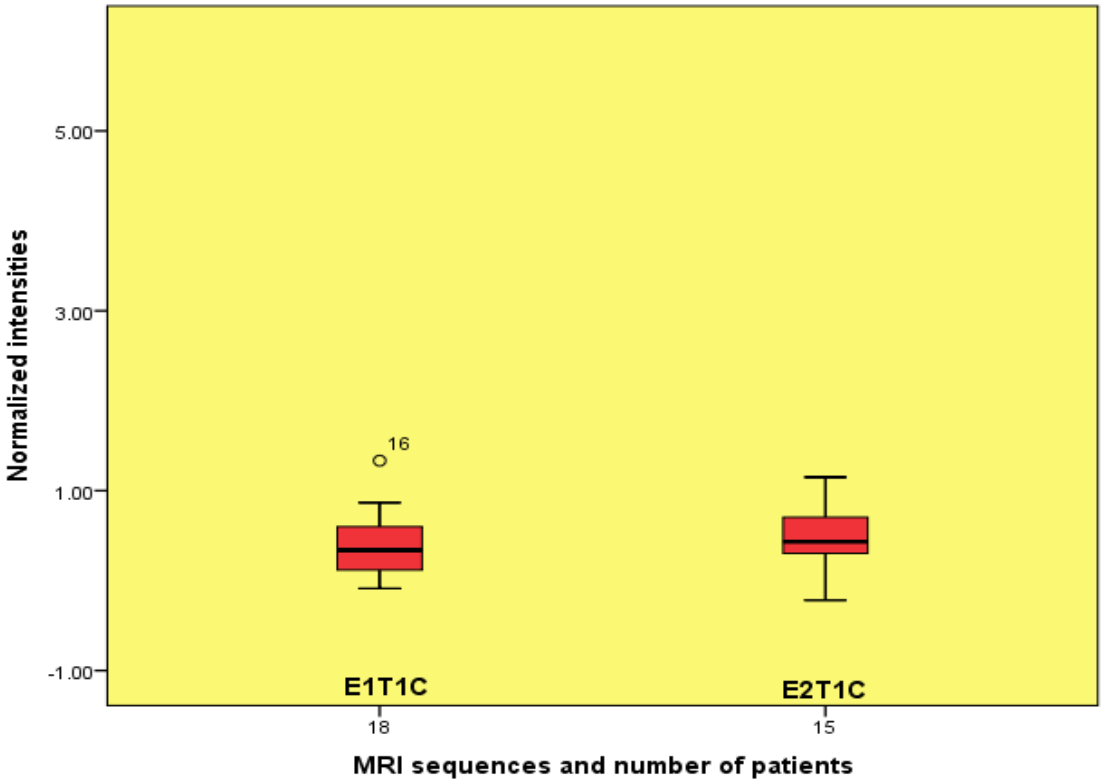

Figure 4.4. Box plot showing the distribution of the normalized mean signal intensities from the T_1WC imaging sequences at time point E1 and E2. T_1WC imaging technique after treatment has a higher contrast ratio than before treatment.

Table 4.7 A descriptive statistic at time point E1and E2 shows that after treatment normalized mean signal intensity is a bit higher than before.

Descriptive Statistics

	N	Minimum	Maximum	**Mean**	Std. Deviation
$E1T_1C$	18	-.09	1.33	**.4186**	.37089
$E2T_1C$	15	-.22	1.15	**.4576**	.37533

Table 4.8 Wilcoxon Signed Ranks Test; there is no statistically significant difference between $E2T_1C \leftrightarrow E1T_1C$.

Wilcoxon Signed Ranks Test

Sequences	$E2T_1C \leftrightarrow E1T_1C$
p value	**0.496**

Comparison between T_2W MRI sequences without fat suppression between the time point E1 and E2

The box plot, figure 4.5, shows that the mean normalized signal intensity distribution for T_2W MRI technique is higher at the time point E1, before treatment, than at time point E2, after treatment. Eighteen patients before treatment and fifteen patients after treatment were analyzed. The mean normalized signal intensities can be seen from table 4.4. The mean normalized signal intensity value before and after treatment can be seen in the table 4.9 below.

A nonparametric statistical analysis, Wilcoxon Signed Ranks Test, is conducted to see if the difference in the mean signal contrast ratio between the pre and post treatment is significant and the result is shown in the table 4.10 below. From the table 4.10 it is clearly seen that the difference is not significant ($p > 0.05$).

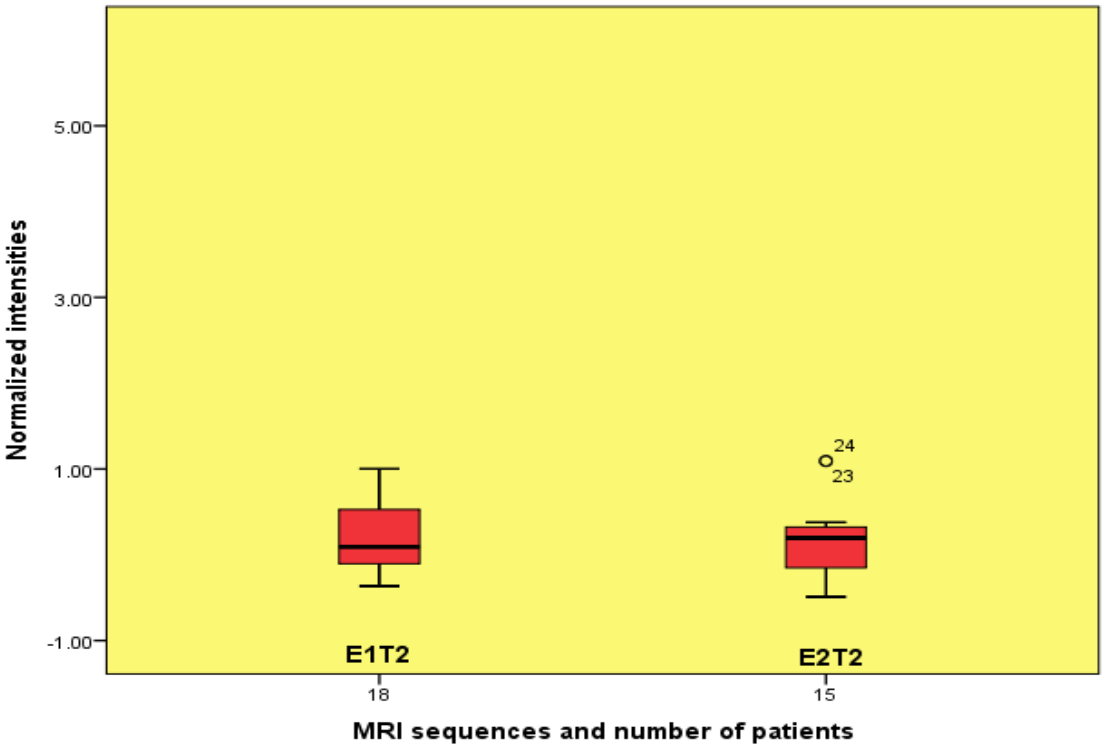

Figure 4.5. Box plot showing the distribution of the normalized mean signal intensities from the T_2W imaging sequences at time point E1 and E2. T_2W imaging technique before treatment has a higher contrast ratio than after treatment.

Table 4.9 A descriptive statistic at time point E1and E2 shows that after treatment the normalized mean signal intensity is less than before.

Descriptive Statistics

	N	Minimum	Maximum	**Mean**	Std. Deviation
$E1T_2$	18	-.37	1.00	**.2119**	.40552
$E2T_2$	15	-.49	1.10	**.1789**	.45011

Table 4.10 Wilcoxon Signed Ranks Test; there is no statistically significant difference between $E2T_2 \leftrightarrow E1T_2$.

Wilcoxon Signed Ranks Test

Sequences	$E2T_2 \leftrightarrow E1T_2$
p value	**0.650**

Comparison between T_2W MRI sequences with fat suppression between the time point E1 and E2

The box plot, figure 4.6, shows that the mean normalized signal intensity distribution for T_2Wfs MRI technique is higher at the time point E1, before treatment, than at time point E2, after treatment. Seventeen patients before treatment and fifteen patients after treatment were analyzed. The mean normalized signal intensity before and after the treatment is shown in the table 4.11.

Once knowing that the mean signal contrast ratio is lower on the T_2Wfs MRI sequence and also in the distribution box plot at the time point E2 than at time point E1, a Wilcoxon Signed Rank Test is conducted to evaluate if this difference is really significant. Table 4.12 shows the output from the Wilcoxon Signed Rank Test and from the table it can be seen that the p value is substantially less than the specified p value of 0.05. This implies that there is significant difference in the normalized signal contrast ratio between the T_2Wfs MRI sequence before and after treatment.

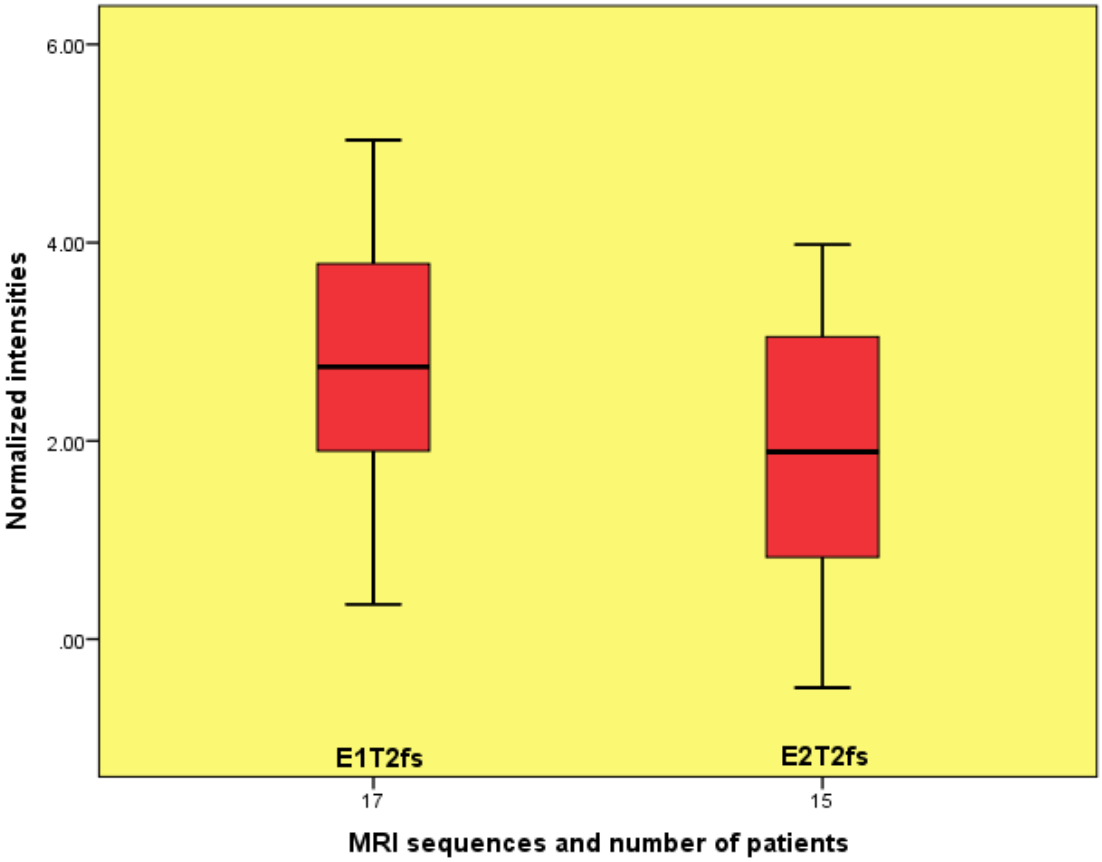

Figure 4.6. Box plot showing the distribution of the normalized mean signal intensities from the T_2Wfs imaging sequences at time point E1 and E2. T_2Wfs imaging technique before treatment has a higher contrast ratio than after treatment.

Table 4.11 A descriptive statistic at time point E1and E2 shows that after treatment the normalized mean signal intensity is less than before.

Descriptive Statistics

	N	Minimum	Maximum	**Mean**	Std. Deviation
$E1T_2fs$	17	.35	5.03	**2.7967**	1.48836
$E2T_2fs$	15	-.49	3.98	**1.8677**	1.38519

Table 4.12 Wilcoxon Signed Ranks Test; there is no statistically significant difference between $E2T_2fs \leftrightarrow E1T_2fs$.

Wilcoxon Signed Ranks Test

Sequences	$E2T_2fs \leftrightarrow E1T_2fs$
p value	**0.006**

5. DISCUSSION

This thesis is part of a big research project work which deals about lymphoma cancer study with different imaging modalities, including ultrasound, CT, PET/CT and MRI. The objective of this preliminary study is to compare the relative conspicuousness of the most common and aggressive NHL, DLBCL on MRI images acquired using pre and post contrast enhanced T_1-weighted, T_2-weighted with and without fat suppression MRI protocols and to analyze the changes between the MRI sequences before and after one week treatment to chemotherapy.

Because of its higher sensitivity towards soft tissues, including neoplasm, MRI imaging is rapidly becoming one of the preferred imaging modalities. In spite of this, there is no clearly defined agreement that states which MRI sequence is best for a specific purpose. Improving the sensitivity of MRI for the detection of aggressive lymphomas, DLBCL, is vital in the diagnostic workup, staging and treatment planning. It is also useful for the better understanding of treatment outcomes in the disease follow-up process.

In this study before and after treatment, the sensitivity of the four MRI sequence was quantitatively evaluated based on the normalized mean signal intensity calculated from the measured signal intensities of the lesion and normal tissues. In addition, this study attempts to see which MRI sequence is better in analyzing the response to chemotherapy in patients with diffuse large B-cell lymphoma. Conclusion was made based on the statistical analyses.

5.1. Comparison between sequences before treatment

The fat suppression MRI sequences are contrast generating sequences that are used to suppress the high signal intensity from fat. This can be achieved by enhancing the signal generated from water containing tissues and nulling the signal from the fat. This is important as most of lesions have high water content. Especially in regions where there is high fat content the fat suppression technique result in the reduction of background signal intensity from the fat and thus the signal from the high water containing lesion will have a high contrast in the dark background and become more conspicuous. Nulling the high signal intensity from the fat will also expand the dynamic range of the image display and enhance the tissue contrast (63). In MRI imaging the signal to noise ratio, SNR, can be improved by decreasing the sampling bandwidth. Though decreasing the bandwidth increases the SNR, it also produces artifacts due to the misplacement of the fat relative to the water. Hence, this increase

in artifact can be eliminated by suppressing the signal from fat which results in overall increase in the image quality from the fat suppression technique (63).

The box plot in the figure 4.1 shows that the T_2W fat suppression MRI protocol has the highest normalized mean signal intensity distribution than the rest of the sequences. The descriptive statistics on table 4.1 also clearly shows the mean signal value of each sequence at time point E1 and T_2Wfs MRI sequence has the highest normalized mean signal value. This implies that the conspicuity level of the lesions at time point E1 on T_2Wfs MRI sequence is much higher than the rest of the sequences. This is supported by the result on the table 4.2 which shows that the mean signal intensity difference between the fat suppression sequence and the rest of the sequences is in a significant level.

Previous studies [60, 62] have also shown that the fat suppression MRI sequences are more sensitive than the conventional spin echo MRI techniques in detecting malignancy, including NHL, of the bone marrow, chest, liver and pelvis before treatment. The result also agrees with the other study [64] which compares the fat suppression MRI sequence with the spin-echo sequence in detecting suspected extreme tumour.The finding of this thesis also agrees with the study on 98 patients with malignant lymphoma of the bone marrow where the fat suppression techniques give a better result in the detection of lymphomatous bone marrow involvement and in the disease staging process than the T_1W spin echo sequence [57].

5.2. Comparison between sequences after treatment

After treatment, at time point E2, the box plot in figure 4.2 shows that the T_2W fat suppression MRI protocol still has the highest normalized mean signal intensity distribution than the rest of the sequences. The descriptive statistics on table 4.3 also clearly shows the mean signal value of each sequence at time point E2 and T_2Wfs MRI sequence has the highest mean signal intensity value. This implies that the conspicuity level of the lesions after treatment on T_2Wfs MRI sequence is still much higher than the rest of the sequences. Moreover this difference between the fat suppression and other sequence after one week treatment is still in significant level.

This finding is in agreement with the study on patients with malignant lymphoma of the bone marrow who are under evaluation of bone marrow transplant after treatment [57]. In this study the fat suppression MRI sequence is compared with the T_1W spin echo sequence for their ability to detect marrow lymphomas and the fat suppression MRI sequence is found to be more superior and also improves the discrimination of marrow sclerosis from tumor.

5.3. Comparison of sequences between time points E1 and E2

Comparison between T_1W MRI sequences before contrast administration between the time points E1 and E2

The T_1 property of a tissue is related to the way how energy is transferred to or absorbed from the surrounding medium of the spinning proton. An efficient transfer of energy results in short T_1 relaxation time. The energy transfer in water molecule is not efficient and hence has long T_1 relaxation time. Tissues with long T_1 relaxation time will have a lower intensity on the T_1W MR image. As tissues that are involved in pathological process often have higher water content than in the normal ones and hence will have lower signal intensity on the T_1W MR image.

During the course of lymphoma treatment the signal intensity of the MR image changes. This is due to the fact that before treatment an active and untreated tumor contains high amount of free water and will have a long T_1 relaxation time which decrease the relative signal intensity of the tumor on the T_1W MR image. After treatment the amount of free water content in the tumor will reduce and be replaced with collagen and fibrotic mass [73]. Hence, T_1 relaxation time will not be solely be because of the water but also the fibrotic mass too. This results in shortening of the T_1 relaxation time than before the treatment and at the same time in increase in the relative signal intensity on the T_1W MR image.

The box plot in figure 4.3 shows an increment in the mean normalized signal intensity distributions after treatment, E2. The descriptive statistics, mean value, on table 4.5 also clearly shows the mean signal value of each sequence before and after treatment. In this study the relative signal intensity has shown increment after one week of treatment cycle. The result on the table 4.6 also shows that there is a significant difference in the mean contrast ratio between the time point E1 and E2. This implies that the treatment has resulted a significant difference after one week.

This result is supported by the previous studies on early treatment response evaluation in patients with diffuse large B-cell lymphoma [16]. On this previous study, the same patients with DLBCL who underwent a standard chemotherapy treatment shows a rapid decrease of both tumor metabolic activity and volume as early as one week after treatment and this was also compared with the PET/CT and provides similar result.

Comparison between T_1W MRI sequences after contrast administration

Clinically, in order to increase the contrast between pathological and normal tissues, contrast enhancement agents are introduced which selectively affect the tissue relaxation times. The Gd-DPTA, a paramagnetic and gadolinium based substance, is one of the commonly used contrast enhancing agents. It has the effect of shortening T_1 relaxation time in tissues where it accumulates and post contrast T_1W image of the tissue will have enhanced signal intensity. In this study Gd-DPTA enhancing is used as a contrast agent before and after treatment. During the treatment cycle the property of the tumour undergoes a change which can be reflected on the MRI images.

From the box plot in figure 4.4, it can be seen that the signal intensity distribution has shown a slight increment after treatment. This is clearly seen in table 4.7 where the mean signal at $E2T_1C$ is a bit higher than at $E1T_1C$. The mean of the change in the mean signal intensity of the pre and post-contrast MR images before and after treatment is calculated from table 4.1 and 4.3; that is the level of enhancement before the treatment and after treatment; and the absolute change in signal intensity in the pre and post-contrast images at time point E1 and E2 is found to be 8.09 and 5.20 respectively. This result indicates that the enhancement is less after treatment and this implies that there is a decrease in the tumor activity after one week of the treatment cycle. Even if there is a change in the tumor activity before and after treatment, this difference is not noticeable in the on the $E2T_1C$. This can be seen on table 4.8 which shows that there is no as such significant difference in signal contrast ratio between the $E2T_1C$ and $E1T_1C$. This is may be due to a short period of treatment follow up, one week. This result agrees with a study [75], on mediastinal masses in Hodgkin's lymphoma patients, which state that the diagnostic accuracy of the MRI based on the intensity enhancement is efficient if it is after 6 months of treatment. The result agrees with a study [77] on mediastinal lymphoma which evaluate the quantitative changes in gadolinium enhancement at MRI imaging after treatment and finds that gadolinium enhancement of the lymphomatous mass has shown a decrease after long term follow up of treatment. This implies that Contrast enhancing method can shows the treatment response of patients to chemotherapy if it is performed after longer treatment follow up. The cost of the contrast agent, the scanning time and the need to acquire the pre contrast T_1 for comparison are some of the limitations of contrast enhanced MRI method and make the method be reserved for cases in which the findings may influence patient management.

Comparison between T_2W MRI sequences without fat suppression

The T_1W MRI images are better in depicting the anatomy of tissues and post contrast T_1W can also be used in delineating pathologic tissues. In spite of this, T_2W MRI images are better than the respective T_1W images in depicting pathologies as most pathologic tissues contain high amount of water than normal tissues and this causes the pathologic tissue to appear more bright than the surrounding tissues [50, 52,55]. Before treatment an active tumor has a characteristic of large water content in the cellular compartment than after treatment. When the proportion of water content reduces after treatment the signal intensity of the tissue on T_2W image will also reduce [77].

In this study the signal intensity has decreased after treatment which is shown in the box plot figure 4.5. The descriptive statistics, mean value, on table 4.9 also clearly shows that the mean signal value of T_2W after treatment is lower than before treatment. Even though there is a decrement in the signal intensity of the T_2W MRI sequence after treatment, the change was not significant as can be seen on table 4.10. As described earlier this could be due to the shorter follow up of the treatment, one week. This result is in agreement with a previous study [77] on the finding of MR changes after treatment on patients with mediastinal lymphoma and the mean signal intensity on the T_2W has shown a decrease after a longer follow up of treatment. Another study [66] on lymphoma of bone marrow has finding that the signal intensity has increase in T_2W after treatment and this may be due to the type of treatment the patient had, radiotherapy, is different than the treatment the patient had in this study, chemotherapy.

Comparison between T_2W MRI sequences with fat suppression

As it is described in the previous results the fat suppression MRI protocols give the highest contrast ratio hence lesion detectability. Because of the reason described above the treatment will have an effect in lowering signal intensity on the T_2Wfs MR images which is clearly seen on the box plot at figure 4.6 and on table 4.11. At the same time these changes before and after treatment were in a significant level as shown in table 4.12. This means that even in a short treatment period the response to treatment is clearly seen on the T_2Wfs MRI and this is beneficial in the treatment response evaluation of patients and follow up to treatment.

Previous study on the same patients with DLBCL has shown that after one week chemotherapy treatment there is a rapid decrease of both tumor metabolic activity and volume which is also compared with the PET/CT and provide similar result. This implies that the T_2W MRI sequence can also provide significant information to treatment response evaluation. This finding is in agreement with the study [61] on

the magnetic resonance imaging of the bone marrow in hematologic malignancies which states that the signal intensity of the marrow on the fat suppression MR images gradually decreases after treatment.

5.4. Reliability of the results

The data's that are used for the analysis were carefully collected as the right slice location and tumor regions is cross checked with diffusion weighted imaging, ADC maps and also with the 3D reconstructed images of the corresponding 2D images.

The choices of the statistical analysis method were also taking into consideration of the number of patients. As the number of patients were small a non-parametric statistical analysis methods were implemented.

The conclusions were made based on the quantitative data which are more powerful than qualitative data's.

The same size of region of interest cannot be taken in the entire patient as lesion especially which are located in the neck regions were small as compared to abdomen or thorax. In addition the conclusion would be stronger if there were visual assessment.

6. CONCLUSIONS

The key finding of this study is that the T_2-weighted with fat suppression sequence is best in detecting lymphoma lesions and evaluating treatment efficacy in patients with DLBCL. This is important because patients are not suppose to go through all the MRI sequences which are so expensive and time taking, in conditions where contrast enhancement is needed. Further clinical studies with large number of patients should be performed to determine the sensitivity and specificity of this technique.

References

[1]. D.D. Brennan, T. Gleeson, L.E. Coate, C. Cronin, D. Carney and S.J. Eustace, A comparison of whole-body MRI and CT for the staging of lymphoma, AJR Am J Roentgenol 185 (2005), pp.711–716.

[2].Torizuka T, Tamaki N, Inokuma T, et al. In vivo assessment of glucose metabolism in hepatocellular carcinoma with FDGPET. J Nucl Med 1995; 36:1811–1817.

[3].Torizuka T, Zasadny KR, Kison PV, Rommelfanger SG, Kaminski MS, Wahl RL. Metabolic response of non-Hodgkin's lymphoma to 131I-anti-B1 radioimmunotherapy: evaluation with FDG PET. J Nucl Med 2000; 41:999–1005.

[4].Weihrauch MR, Re D, Scheidhauer K, et al. Thoracic positron emission tomography using 18F-fluorodeoxyglucose for the evaluation of residual mediastinal Hodgkin disease. Blood 2001; 98:2930–2934.

[5].Schoder H, Noy A, Gonen M et al (2005) Intensity of 18fluorodeoxyglucose uptake in positron emission tomography distinguishes between indolent and aggressive non-Hodgkin's lymphoma. J Clin Oncol 23:4643–4651.

[6].Spaepen K, Stroobants S, Dupont P et al (2002) Early restaging positron emission tomography with (18)F-fluorodeoxyglucose predicts outcome in patients with aggressive non-Hodgkin's lymphoma. Ann Oncol 13:1356–1363.

[7].Ngeow JY, Quek RH, Ng DC et al (2009) High SUV uptake on FDGPET/CT predicts for an aggressive B-cell lymphoma in a prospective study of primary FDG-PET/CT staging in lymphoma. Ann Oncol 20:1543–1547.

[8].Braams JW, Pruim J, Freling NJ et al (1995) Detection of lymph node metastases of squamous cell cancer of the head and neck with FDG-PET and MRI. J Nucl Med 36:211–216.

[9].Juweid ME, Stroobants S, Hoekstra OS, Mottaghy FM, Dietlein M, Guermazi A, Wiseman GA, Kostakoglu L, Scheidhauer K, Buck A, Naumann R, Spaepen K, Hicks RJ, Weber WA, Reske SN, Schwaiger M, Schwartz LH, Zijlstra JM, Siegel BA, Cheson BD. Use of positron emission tomography for response assessment of lymphoma: consensus of the Imaging Subcommittee of International Harmonization Project in Lymphoma. J. Clin. Oncol. 2007; 25: 571–578.

[10].Cheson BD, Horning SJ, Coif?er B, Shipp MA, Fisher RI, Connors JM, Lister TA, Vose J, Grillo-Lopez A, Hagenbeek A, Cabanillas F, Klippen-sten D, Hiddemann W, Castellino R, Harris NL, Armitage JO, Carter W,Hoppe R, Canellos GP. Report of an international workshop to standardize response criteria for non-Hodgkin's lymphomas. NCI Sponsored International Working Group. J. Clin. Oncol.1999; 17:1244–1253.

[11].Plathow C, Walz M, Lichy MP, Aschoff P, Pfannenberg C, Bock H, Eschmann SM, Claussen CD, Schlemmer HP. Cost considerations for whole-body MRI and PET/CT as part of oncologic staging. Radiology 2008; 48:384-396.

[12].Surveillance computed tomography scans for patients with lymphoma: is the risk worth the benefits? Pareen Shenoy, Rajni Sinha, John W Tumeh, Mary Jo Lechowicz, Christopher R Flowers in Clinical lymphoma myeloma leukemia (2010).

[13].Huang B, Law MW, Khong PL. Whole-Body PET/CT Scanning: Estimation of Radiation Dose and Cancer Risk.

[14].Wu, X., Kellokumpu-Lehtinen, P.-L., Pertovaara, H., Korkola, P., Soimakallio, S., Eskola, H. and Dastidar, P. (2011), Diffusion-weighted MRI in early chemotherapy response evaluation of patients with diffuse large B-cell lymphoma a pilot study: comparison with 2-deoxy-2-fluoro-D-glucose-positron emission tomography/computed tomography.NMR in Biomedicine.

[15].Schmidt GP, Haug A, Reiser MF, Rist C.Whole-body MRI and FDG-PET/CT imaging Diagnostics in oncology. Radiologe. 2010 Apr; 50(4):329-38.

[16].Wu X, Dastidar P, Pertovaara H, Korkola P, Jarvenpaa R, Rossi M,Koobi T, Eskola H, Kellokumpu-Lehtinen PL. Early treatment response evaluation in patients with diffuse large B-cell lymphoma – a pilot study comparing volumetric MRI and PET/CT. Mol. Imaging Biol. 2010, DOI: 10.1007/s11307-010-0404-z.

[17].Harrison L, Luukkaala T, Pertovaara H, Saarinen T, Heinonen T, Järvenpää R, Soimakallio S,Kellokumpu-Lehtinen P, Eskola H, Dastidar P: Non-Hodgkin lymphoma response evaluation with MRI texture classification. Journal of Experimental & Clinical Cancer Research 2009, 28:87-100.

[18].Koh DM, Collins DJ. Diffusion-weighted MRI in the body: applications and challenges in oncology. AJR Am J Roentgenol. 2007;188(6):1622–1635.

[19].Roman, E. and Smith, A. G. (2011), Epidemiology of lymphomas. Histopathology, 58: 4–14. doi: 10.1111/j.1365-2559.2010.03696.x

[20].Yung L, Linch D. Hodgkin's lymphoma. Lancet 2003; 361: 943–951.

[21].Ekstrom-Smedby K (2006) Epidemiology and Etiology of non-Hodgkin lymphoma a review. Acta Oncol 45:258–271

[22].Deborah.T , Nancy.E.K, Editor (2010), Pediatric Oncology Nursing: Advanced Clinical Handbook, Springer, 2010.

[23].Dalla-Favera R, Gaidano G. Molecular biology of lymphomas. In: DeVita VTJ, Hellman S, Rosenberg SA, eds. Cancer: principles and practice of oncology. Philidelphia: Lippincott Williams, and Wilkins; 2001: 2215–35.

[24]. Evans LS, Hancock BW. Non-Hodgkin lymphoma. Lancet 2003;362:139–46.

[25]. Clarke C,O'malley C. Non-Hodgkin lymphoma.In: RiesLAG,YongJL, KeelGE, EisnerMP, LinYD, HornerM-JD, editors. Cancer Survival Among Adults: US SEER Program, 1988–2001, Patient and Tumor Characteristics. Bethsda, MD: National Cancer Institute's, SEER Program, NIH; 2007. pp 235–242, Chapter 28.

[26]. Patte C: Non-Hodgkin's lymphoma. Eur J Cancer 34:359-362, 1998

[27]. American Cancer Society. 2010 .Non Hodgkin Lymphoma July 20, 2011.

[http://documents.cancer.org/acs/groups/cid/documents/webcontent/003126-pdf.pdf]

[28]. Fong D, Steurer M, Greil R, et al: Hodgkin lymphoma in Tyrol – a population-based study. Ann Hematol 2009;88:449–456.

[29]. Ansell SM, Armitage J. Non-Hodgkin lymphoma: diagnosis and treatment. Mayo Clin Proc 2005; 80: 1087–1097.

[30].Michael L. G, Malignant Lymphomas. BC Decker Inc (2002): 67-83

[31].Rogers, B.B. Overview of Non-Hodgkin's Lymphoma (2006) Seminars in Oncology Nursing, 22(2), pp. 67-72.

[32].Ansell SM, Armitage J Non-Hodgkin lymphoma: diagnosis and treatment. Mayo Clin Proc 2005;80:1087-1097.

[33].Kwee TC, Kwee RM, Nievelstein RA. Imaging in staging of malignant lymphoma: a systematic review. Blood. 2008;111(2):504–516.

[34].Gossmann A, Eich HT, Engert A, Josting A, Müller RP, Diehl V, Lackner KJ. CT and MR imaging in Hodgkin's disease--present and future. Eur J Haematol Suppl. 2005;31:83–89.

[35].Castellino RA, Blank N, Hoppe RT, et al. Hodgkin disease: contributions of chest CT in the initial staging evaluation. Radiology 1986;160:603–5.

[36].Hopper KD, Diehl LF, Lesar M, et al. Hodgkin disease: clinical utility of CT in initial staging and treatment. Radiology 1988;169:17–22.

[37].Romano M, Libshitz HI. Hodgkin disease and non-Hodgkin lymphoma: plain ches radiographs and chest computed tomography of thoracic involvement in previously untreated patients. Radiol Med (Torino) 1998;95:49–53.

[38].Raanani P, Shasha Y, Perry C. Is CT scan still necessary for staging in Hodgkin and non-Hodgkin lymphoma patients in the PET/CT era? Ann Oncol 2006; 17: 117–22

[39].Lucey BC, Stuhlfaut JW, Soto JA. Mesenteric lymph nodes: detection and significance on MDCT. AJR Am J Roentgenol. 2005;184:41-44.

[40].Lin M (2011) Molecular imaging using positron emission tomography in colorectal cancer. Discov Med 11(60):435–447.

[41].Wiedmann E, Baican B, Hertel A, et al. Positron emission tomography (PET) for staging and evaluation of response to treatment in patients with Hodgkin's disease. Leuk Lymphoma 1999; 34:545–51.

[42].Rege S, Maass A, Chaiken L et al (1994) Use of positron emission tomography with fluorodeoxyglucose in patients with extracranial head and neck cancers. Cancer 73:3047–3058.

[43].Kazama T, Faria SC, Varavithya V, et al. FDG PET in the evaluation of treatment for lymphoma: clinical usefulness and pitfalls. Radiographics. 2005; 25(1):191–207.

[44].Abouzied MM,Crawford ES,Nabi HA. 18F-FDG imaging: pitfalls and artifacts. J Nucl Med Technol 2005;33(3):145–155.

[45].la Fougere C, Hundt W, Brockel N, et al. Value of PET/CT versus PET and CT performed as separate investigations in patients with Hodgkin's disease and non-Hodgkin's lymphoma. Eur J Nucl Med Mol Imaging. July 21, 2006.

[46].Rahmouni A, Luciani A, Itti E. MRI and PET in monitoring response in lymphoma. Cancer Imaging. 2005;5(A):S106–12

[47].Tatsumi M, Cohade C, Nakamoto Y, Fishman EK, Wahl RL. Direct comparison of FDG PET and CT findings in patients with lymphoma: initial experience. Radiology. 2005; 237:1038–1045.

[48].Landis K. Griffeth, Use of PET/CT scanning in cancer patients: technical and practical considerations, bumcrproceedings (2005); 18:321-330.

[49].Jacobs MA, Ibrahim TS, Ouwerkerk R. AAPM/RSNA physics tutorials for residents: MR imaging: brief overview and emerging applications. Radiographics. 2007;27(4):1213–1229.

[50]. Westbrook C. MRI at a glance. Oxford, England: Blackwell Science, 2002.

[51].Timothy, L. & Christopher, K.(2004), Biomedical technology and devices handbook. United States of America: CRC Press LLC (pp.208-236).

[52].Hashemi RH, Bradley WG. MRI: The Basics. Baltimore, MD: Lippincott Williams & Wilkins; 1997.

[53].Stephen K., Magnetic resonance imaging in medicine Phys. Educ.2001; 36 476

[54].Rofsky NM, Lee VS, Laub G, et al. Abdominal MR imaging with a volumetric interpolated breath-hold examination. Radiology 1999; 212:876-884.

[55].Bitar R, Leung G, Perng R, Tadros S, Moody AR, Sarrazin J, McGregor C, Christakis M, Symons S, Nelson A, Roberts TP. MR pulse sequences: what every radiologist wants to know but is afraid to ask. Radiographics. 2006;26:513-37.

[56].Kataoka M, Ueda H, Koyama T et al (2005) Contrast-enhanced volumetric interpolated reath-hold examination compared with spin-echo T_1-weighted imaging of head and neck tumors. AJR Am J Roentgenol 184:313–319.

[57].Hoane BR, Shields AF, Porter BA, Shulman HM (1991) Detection of lymphomatous bone marrow involvement with magnetic resonance imaging. Blood 78:728–738.

[58].Gossmann A, Eich HT, Engert A, Josting A, Müller RP, Diehl V, Lackner KJ. CT and MR imaging in Hodgkin's disease--present and future. Eur J Haematol Suppl 2005; 83-89.

[59].Coller BS, Chabner BA, Gralnick HR. Frequencies and patterns of bone marrow involvement in non-Hodgkin lymphomas: observations on the value of bilateral biopsies. AmJ Hematol 1977;3:105–119.

[60]. ShumanWP, Baron RL, Peters MJ, Tazioloi PK. Comparison of STIR and spin-echo MR imaging at 1.5 T in 90 lesions of the chest, liver, and pelvis. AJR Am J Roentgenol1989;152(4):853–859.

[61].Moulopoulos L, Dimopoulos M. Magnetic resonance imaging of the bone marrow in hematologic malignancies. Blood 1997; 90:2127-2147.

[62].Mirowitz S, Apicella P, Reinus WR, Hammerman AM: MR imaging of bone marrow lesions: Relative conspicuousness on T_1- weighted, fat-suppressed T_2-weighted, and STIR images. AJR Am J Roentgenol 162:215, 1994.

[63] Mitchell DG, Vinitski S, Rifkin MD, Burk DL Jr. Sampling bandwidth and fat suppression: effects on long TR/TE MR imaging of the abdomen and pelvis at 1.5 T. Am J Roentgenol 1989; 153: 419–425.

[64] Shuman WP, Pattern RM, Baron RL, Liddel RM, Conrad EU, Richardson ML. Comparison of STIR and spin-echo MR imaging at 1.5 T in 45 suspected extremity tumors: lesion conspicuity and extent. Radiology 1991; 179:247-252.

[65]. DelfautEM, Beltran J, Johnson G, Rousseau J, Marchandise X, Cotten A. Fat suppression in MR imaging: techniques and pitfalls. RadioGraphics1999; 19: 373–382.

[66] . Hwang, S. and D. M. Panicek . Magnetic resonance imaging of bone marrow in oncology, Part 2. Skeletal Radiol 36:1017–1027. 2007.

[67].Colosimo C, Cianfoni A, Di Lella GM, Gaudino S. Contrast-enhanced MR imaging of the spine: when, why and how? How to optimize contrast protocols in MR imaging of the spine. Neuroradiology 2006;48 (Suppl 1):18–33.

[68].I.S. Haldorsen, A. Espeland, and E.-M. Larsson Central Nervous System Lymphoma:Characteristic Findings on Traditional and Advanced Imaging AJNR Am.J Neuroradiol. 2011 32: 984-992.

[69].Johnson BA, Fram EK, Johnson PC, Jacobowitz R. The variable MR appearance of primary lymphoma of the central nervous system: comparison with histopathologic features. AmJ Neuroradiol 1997 ;18 :563-572.

[70].Eloraby A, Zaki I. Primary central nervous system lymphoma: incorporating MRI in the planning of treatment strategies. Journal of the Egyptian Nat.Cancer Inst.;Vol. 13, No. 3,September, 237-244,2001.

[71].Thurnher MM, Thurnher SA, Fleischmann D, et al. Comparison of T_2-weighted and fluid-attenuated inversion-recovery fast spin-echo MR sequences in intracerebral AIDS-associated disease. AJNR Am J Neuroradiol 1997;18:1601-1609.

[72].Thurnher MM, Rieger A, Kleibl-Popov C et al. (2001). Primary central nervous system lymphoma in AIDS: a wider spectrum of CT and MRI findings. Neuroradiology 43: 29–35.

[73].Go JL, Lee SC, Kim PE. Imaging of primary central nervous system lymphoma. Neurosurg Focus 2006;21:E4.

[74].Bonomo L, Ciccotosto C, Guidotti A, Merlino B Storto ML (1997) Staging of thoracic lymphoma by radiological imaging. Eur Radiol 7 :1179–1189.

[75].Di Cesare E, Cerone G, Enrici RM, Tombolini V, Anselmo P, Masciocchi C. MRI characterization of residual mediastinal masses in Hodgkin's disease: long-term follow-up. Magn Reson Imaging 2004; 22:31-38

[76].Bittner RC, Felix R. Magnetic resonance (MR) imaging of the chest: state of the art. Eur Respir J 1998; 11: 1392–1404.

[77].Rahmouni A, Divine M, Lepage E, et al. Mediastinal lymphoma: quantitative changes in gadolinium enhancement at MR imaging after treatment. Radiology 2001; 219:621–628.

[78].Reimer P, Parizel PM, Stichnoth FA, Meaney JF. Clinical MR Imaging: A Practical Approach. Springer 2010: 493–516

[79].Q. Chen, K.W. Stock, P.V. Prasad and H. Hatabu, Fast magnetic resonance imaging techniques, Eur J Radiol 29 (1999), pp. 90–100.

[80].Vanel D, Dromain C, Tardivon A (2000) MRI of bone marrow disorders. Eur Radiol 10:224–229.

[81].Daldrup-Link HE, Franzius C, Link TM et al (2001) Whole-body MR imaging for detection of bone metastases in children and young adults: comparison with skeletal scintigraphy and FDG PET. Am J Roentgenol 177:229–236.

[82].Brennan DD, Gleeson T, Coate LE, et al. A comparison of whole-body MRI and CT for the staging of lymphoma. AJR. 2005;185:711–716.

[83].Kellenberger CJ, Miller SF, Khan M et al (2004) Initial experience with FSE STIR whole-body MR imaging for staging lymphoma in children. Eur Radiol 14:1829–1841.

[84].Hoane BR, Shields AF, Porter BA, Borrow JW (1994) Comparison of initial lymphoma staging using computed tomography (CT) and magnetic resonance (MR) imaging. Am J Hematol 47:100–105.

[85].Greco A, Jelliffe AM, Maher EJ, Leung AW (1988) MR imaging of lymphomas: impact on therapy. J Comput Assist Tomogr 12:785–791.

[86].Mehta RC,Marks MP, Hinks RS, Glover GH, Enzmann DR. MR evaluation of vertebral metastases: T_1-weighted short inversion time inversion recovery, fast spin echo, and inversion-recovery fast spin-echo sequences. Am J Neuroradiol 1995;16:281–8.

[87].Schmidt G, Dinter D, Reiser MF, Schoenberg S. Clinical MR Imaging: A Practical Approach. Springer 2010: 763-788.

[88].Li S, Xue HD, Li J et al (2008) Application of whole body diffusion weighted MR imaging for diagnosis and staging of malignant lymphoma. Chin Med Sci J 23:138–144.

[89].D.–M. Koh, H.C. Thoeny, Editors, Diffusion–Weighted MR Imaging: Applications in the Body, Berlin, Heidelberg: Springer–Verlag, 2010.

[90].Kwee T C, Takahara T, Vermoolen M A, Bierings M B, Mali W P, Nievelstein R A J. Whole-body diffusion-weighted imaging for staging malignant lymphoma in children. Pediatr Radiol. 2010.

[91].Mori, S. and Barker, P. B. (1999), Diffusion magnetic resonance imaging: Its principle and applications. The Anatomical Record, 257: 102–109.

[92].Perrone A, Guerrisi P, Izzo L, D'Angeli I, Sassi S, Mele LL, Marini M, Mazza D, Marini M. Diffusion-weighted MRI in cervical lymph nodes: differentiation between benign and malignant lesions. Eur. J. Radiol. 2011; 77: 281–286.

[93].Holzapfel K, Duetsch S, Fauser C, Eiber M, Rummeny EJ, Gaa J. Value of diffusion-weighted MR imaging in the differentiation between benign and malignant cervical lymph nodes. Eur. J.Radiol.2009; 72: 381–387.

[94].Lu JJ, Brady LW (2008) Radiation Oncology. An Evidence-Based Approach. Springer, Heidelberg.

[95]. Rossi M. 2011. Magnetic Resonance Image Segmentation and Signal Analysis for Medical Applications. Doctoral Science Thesis. Tampere, Tampere university of technology. 53p.